Comparative analysis of the syncytiotrophoblast in placenta tissue and trophoblast organoids using snRNA sequencing

Madeline M Keenen[1], Liheng Yang (杨利恒)[2], Huan Liang[1,3], Veronica J Farmer[1], Rizban E Worota[2], Rohit Singh[1,3], Amy S Gladfelter[1]*, and Carolyn B Coyne[2,4]*

1) Duke University School of Medicine, Department of Cell Biology, Durham, NC
2) Duke University School of Medicine, Department of Integrative Immunobiology, Durham, NC
3) Duke University School of Medicine, Department of Biostatistics and Bioinformatics
4) Duke Human Vaccine Institute, Durham, NC

*Address correspondence:

Carolyn Coyne, PhD
3130 Medical Sciences Research Building III
3 Genome Court
Durham, NC 27710
USA
carolyn.coyne@duke.edu

Amy Gladfelter, PhD
C351 LSRC
308 Research Drive
Durham, NC 27708
USA
amy.gladfelter@duke.edu

Abstract

The outer surface of chorionic villi in the human placenta consists of a single multinucleated cell called the syncytiotrophoblast (STB). The unique cellular ultrastructure of the STB presents challenges in deciphering its gene expression signature at the single-cell level, as the STB contains billions of nuclei in a single cell. There are many gaps in understanding the molecular mechanisms and developmental trajectories involved in STB formation and differentiation. To identify the underlying control of the STB, we performed comparative single nucleus (SN) and single cell (SC) RNA sequencing on placental tissue and tissue-derived trophoblast organoids (TOs). We found that SN RNA sequencing was essential to capture the STB population from both tissue and TOs. Differential gene expression and pseudotime analysis of TO-derived STB identified three distinct nuclear subtypes reminiscent of those recently identified *in vivo*. These included a juvenile nuclear population that exhibited both CTB and STB marker expression, a population enriched in genes involved in oxygen sensing, and finally a subtype enriched in transport and GTPase signaling molecules. Notably, suspension culture conditions of TOs that restore the native orientation of the STB (STB^{out}) showed elevated expression of canonical STB markers and pregnancy hormones, along with a greater proportion of the STB nucleus subtype specializing in transport and GTPase signaling, compared to those cultivated with an inverted STB polarity (STB^{in}). Gene regulatory analysis identified novel markers of STB differentiation conserved in tissue and TOs, including the chromatin remodeler RYBP, that exhibited STB-specific RNA and protein expression. CRISPR/Cas9 knockout of RYBP in STB^{in} TOs did not impact cell-cell fusion; however, bulk RNA sequencing revealed downregulation of the pregnancy hormone CSH1 and upregulation of multiple genes associated with the oxygen-sensing STB nuclear subtype. Finally, we compared STB gene expression signatures amongst first trimester tissue, full-term tissue, and TOs, identifying many commonalities but also notable variability across each sample type. This indicates that STB gene expression is responsive to its environmental context. Our findings emphasize the utility of TOs to accurately model STB differentiation and the distinct nuclear subtypes observed *in vivo*, offering a versatile platform for unraveling the molecular mechanisms governing STB functions in placental biology and disease.

Introduction

During the course of human gestation, the developing fetus forms an entire external organ to support its growth—the placenta. While the fetal organs undergo development, the placenta assumes a multifaceted role, serving to facilitate molecular exchange, perform essential metabolic functions, produce hormones, prevent loss of immune tolerance, and act as a barrier against the vertical transmission of pathogens (Aye et al., 2022; Benirschke et al., 2012; Costa, 2016; Megli and Coyne, 2021). The placenta's remarkable functional complexity is underscored by its distinctive cellular architecture. Its outer layer encompasses a giant single cell called the syncytiotrophoblast (STB), that contains billions of nuclei and envelops the chorionic villi (Barker et al., 1973; Burton and Jauniaux, 1995; Haeussner et al., 2014). The STB is formed via cell-cell fusion of the underlying cytotrophoblast (CTB) cell population. CTBs reside on the basement membrane of chorionic villi to contribute new nuclei into the STB or lie at the interface between the placenta villi and the maternal decidua in multi-cell layered structures termed cell columns (CTB-CC) (**Figure 1A**) (Boyd and Hamilton, 1970). CTBs closer to the maternal decidua are more differentiated than their counterparts lower in the column and eventually undergo epithelial to mesenchymal transition (EMT) to form fully differentiated extravillous trophoblast cells (EVT) that invade into the decidua (**Figure 1A**) (Arutyunyan et al., 2023; Turco and Moffett, 2019). The molecular mechanisms and environmental cues that drive CTB differentiation into either STB or EVT lineages is an area of active research and defining these trajectories are essential to understand placenta development and pathogenesis.

Several groups have applied single-cell RNA sequencing (SC) of primary tissue throughout gestation, trophoblast organoids (TOs), and trophoblast stem cells (TSCs) to characterize EVT differentiation (Arutyunyan et al., 2023; Li et al., 2024; Liu et al., 2018; Marsh et al., 2022; Pique-Regi et al., 2019; Shannon et al., 2024; Suryawanshi et al., 2018; Vento-Tormo et al., 2018). This has generated a lineage map of CTB-to-EVT differentiation with identification of its terminal states and the potential transcription factors involved. However, these datasets contain very few cells from the STB, limiting characterization of the CTB-to-STB differentiation process. This scarcity likely arises because the STB, being a large single cell, is excluded during the single-cell isolation and size filtration steps required for the 10x Genomics microfluidics pipeline. Therefore, approaches like single nucleus RNA sequencing (SN) may be essential to properly capture the heterogeneity of STB gene expression. In fact, a recent study performed SN on placenta tissue (six first trimester and six full-

96 term tissues) and captured STB nuclei and defined their lineage trajectories at each gestational age (Wang et
97 al., 2024). Their analysis suggests the STB can bifurcate into at least two nuclear lineages post-fusion,
98 associated with either hormone expression and GTPase signaling or with an oxygen response. This implies
99 different functions of the STB may be attributed to distinct individual nuclei within the same giant cell. However,
100 how nuclei with distinct gene expression arise and how they impact the function of the entire STB cell is not
101 known. Dissecting nuclear heterogeneity in the STB will require a molecular biology and genetic toolkit that has
102 been largely inaccessible for human pregnancy models.

103 A major challenge in establishing genetically tractable and accessible models for the human placenta
104 is the remarkable diversity of placental structures amongst mammals, and notably the variations in the tissue
105 architecture and cell types seen even between humans and mice (Hemberger et al., 2020; Wooding and Burton,
106 2008). In the last several years, trophoblast organoids (TOs) have emerged as powerful tools for studying
107 trophoblast differentiation. CTB progenitor cells can be isolated from tissue throughout gestation, as CTB
108 remain mitotic throughout pregnancy (Haider et al., 2018; Mayhew, 2014; Turco et al., 2019; Yang et al., 2022).
109 They can subsequently be maintained in a proliferative state capable of trophoblast differentiation by using a
110 growth factor cocktail and cultivation in extracellular matrix (Okae et al., 2018; Turco et al., 2019; Yang et al.,
111 2022), and spontaneously fuse to form STB (Haider et al., 2018; Li et al., 2023; Turco et al., 2019; Yang et al.,
112 2022). In standard culture conditions, TOs exhibit an inverted architecture compared to placental villi *in vivo*,
113 with an outward facing proliferative CTB layer and a largely inward facing STB (STB^{in}) (Haider et al., 2018;
114 Turco et al., 2019; Yang et al., 2022). Our recent work has established a method to reverse the cellular polarity
115 of TOs to their native orientation, resulting in organoids containing very large (>50 nuclei) STB on the outermost
116 layer and mononuclear CTBs positioned in the center (STB^{out}), and exhibit increased secretion of the STB-
117 associated hormone human chorionic gonadotropin (hCG) (Yang et al., 2023). Recapitulating the native
118 orientation of outward facing STB is essential to model key aspects of STB function *in vitro*, such as molecular
119 transport and its role as a barrier to infection and immune cells. However, how changes in TO orientation affect
120 the functional differentiation of STB remains an important and unexplored area of investigation. While the
121 majority of CTBs in TOs differentiate into the STB, a small proportion can spontaneously differentiate into HLA-
122 G^+ EVTs. This EVT percentage can be increased through a three-step treatment involving Neuregulin-1 (NRG1)

123 (EVT^{enrich}) (Haider et al., 2018; Turco et al., 2019; Yang et al., 2022). Consequently, TOs offer the ability to
124 induce differentiation along both STB and EVT lineages and have rapidly become a powerful and accessible
125 tool to investigate trophoblast biology.

126 As TOs become increasingly prevalent as a research model, it is crucial to assess their resemblance to
127 *in vivo* trophoblast cell types. Further, the gene expression signature of the STB and any heterogeneity that
128 exists amongst nuclei remains enigmatic due to its unique multinucleated ultrastructure, both i*n vitro* and *in*
129 *vivo*. In this study, we performed comparative SC and SN on primary full-term placenta tissue and TOs. We
130 found that SN is essential to capture STB gene expression both in tissue and TOs, while SC enriches for mitotic
131 cells, maternal immune cells, and EVT cells in tissue. Differential gene expression and pseudotime analysis of
132 distinct STB nuclei in TOs identified three distinct subtypes reminiscent of those recently identified *in vivo*: a
133 juvenile population that exhibits both CTB and STB expression, an FLT1-expressing population enriched in
134 genes involved in oxygen sensing, and a subtype enriched in expression of molecular transport and GTPase
135 signaling molecules. While STB^{in} and STB^{out} conditions maintain a similar proportion of CTB cell nuclei, STB^{out}
136 TOs exhibited a higher proportion of the transport and GTPase STB-3 nuclear subtype while STB^{in} exhibited a
137 higher proportion of the oxygen sensing STB-2 subtype. Pseudotime and gene regulatory network analysis of
138 RNA velocity identified genes linked to STB differentiation, including the chromatin effector RYBP which is
139 enriched in STB^{out} TOs. To validate this analysis, we utilized CRISPR/Cas9 to knock-out RYBP in TOs. We
140 found that deletion of RYBP in STB^{in} TOs did not affect cell-cell fusion or STB formation, but bulk RNA
141 sequencing demonstrated that RYBP KO resulted in a significant decrease in the expression of the pregnancy
142 hormone CSH1 and an increase in expression of key genes that define the oxygen sensing STB-2 nuclear
143 subtype. Finally, STB gene expression was compared between TOs and primary tissue at different stages of
144 gestation. The CTBs were remarkably similar across all conditions, indicating that CTBs isolated from term
145 placenta that are used for TO generation are comparable to those isolated at earlier stages of pregnancy. The
146 STB displayed both commonalities and notable variability across the sample types. Together, this work
147 demonstrates the capacity of TOs to mirror STB differentiation and the nuclear subtypes seen *in vivo*, providing
148 an accessible platform to dissect the key molecular pathways underlying placenta function, distinct STB
149 subtypes, and trophoblast-related pregnancy disorders.

150 **Results**

151 **Single nucleus sequencing is necessary to capture the gene expression signature of STBs in placental**
152 **tissue and TOs**

153 In this study, we set out to compare the transcriptional profile of full-term placental tissue composed of
154 placental villi and decidua (**Figure 1A, 1B**) to STB^{in} TOs previously derived from placental tissue (**Figure 1B**).
155 To assess whether SC or SN sequencing could effectively capture trophoblast cell populations, we processed
156 matched samples into single cells/syncytial fragments or single nuclei (**Figure 1C, Materials and Methods**).
157 The SC and SN datasets generated from primary placental tissue (**Figure 1 D-F**) and TOs (**Figure 1 G-I**) were
158 integrated, and a graph-based clustering approach used to identify clusters (Butler et al., 2018; Hao et al.,
159 2021; Satija et al., 2015; Stuart et al., 2019). Each dataset was visualized with a UMAP plot (**Figure 1D** and
160 **1G**) and established gene expression markers were used to determine the cell or nuclear identity of each
161 cluster (**Figure 1F**, **1I**, **Supplementary Figure 1.1C and 1.1F, and Supplemental Table 1-2**) (Arutyunyan et
162 al., 2023; Derisoud et al., 2024; Vento-Tormo et al., 2018).

163 To determine how each sequencing technique affects the detection of trophoblast cell types, we first
164 defined the cell/nucleus types in the primary tissue dataset. We identified two CTB clusters, seven STB clusters,
165 and two EVT clusters, each expressing their respective markers (e.g., PAGE4, CYP19A1, and HLA-G) (**Figure**
166 **1D, 1F, Supplemental Figure 1.1C**). The clusters for each cell type are labeled with a randomly ordered
167 number. There was a similar distribution of these subtypes across all three donor tissues (**Supplemental**
168 **Figure 1.1A-B**). As in previous single cell approaches, our SC tissue dataset captured only a small fraction of
169 the STB cell type (6% of total cells are STB). In contrast, the predominant population in the SN preparation was
170 STB nuclei, accounting for 76% of the total nuclei count, (**Figure 1D-1E** and **Supplemental Figure 1.1A-B**)
171 and consistent with their relative prevalence *in vivo* (Mayhew, 2014; Mayhew and Simpson, 1994; Simpson et
172 al., 1992). Specifically, the SN dataset on primary tissue had an 8:1 ratio of STB to CTB, resembling
173 stereological estimates of placental trophoblast compositions at full-term (9:1) indicating that enzymatic
174 digestion of nuclei is capturing a representative population of these trophoblast nucleus types. (**Figure 1D**).
175 While the STB subtype is better captured by SN sequencing, SC sequencing exhibited significant enrichment
176 in both EVT (18% of total in SC vs. 1.3% in SN) and macrophages (53% of total in SC vs. 1.9% in SN) (**Figure**

177 **1D-1E** and **Supplemental Figure 1.1A-B)**. As a control for SC/SN dataset integration, cell/nucleus types were
178 identified within the individual SC and SN datasets and proportions mirrored the integrated SC/SN dataset
179 (**Supplemental Figure 1.2 and 1.3**). Thus differences between tissue processing for either SC or SN impact
180 the cell types that can be recovered and subsequently sequenced and SN is essential for the analysis of the
181 STB.

182 We next defined the nucleus types represented in the STB^{in} TO dataset, in which we identified two
183 proliferating CTB clusters (CTB-p), five non-proliferative CTB clusters (CTB-1-5), one pre-fusion CTB cluster
184 with high expression of endogenous retroviral fusion genes (CTB-pf), and two STB clusters (STB 1-2) (**Figure**
185 **1G-1I** and **Supplemental Figure 1.1F**). The clusters for each cell type are labeled with a randomly assigned
186 number and color, and therefore cluster numbers and color for each cell type cannot be directly compared
187 between the tissue and TO individual datasets until they are integrated in Figure 6. Like placenta tissue, the
188 SC dataset captured only a small number of the total STB present in TOs, with only 2.4% of the total cell
189 population attributed to the STB (**Figure 1G** and **Supplemental Figure 1.1E**). In contrast, the STB accounted
190 for 38% of the total nuclear numbers captured by SN sequencing (**Figure 1G** and **Supplemental Figure 1.1E**).
191 The differences in non-proliferative CTB populations (CTB 1-5) between SC and SN sequencing were less
192 pronounced, with 57% of the total cell population from SC sequencing attributed to these cells and 56% of
193 nuclei in the SN dataset (**Figure 1G** and **Supplemental Figure 1.1E**). Similarly, both SC and SN captured
194 nearly identical numbers of CTB-pf cells (7%). However, the number of CTB-p were only 16% of the total
195 population in SN despite accounting for 40% in SC, consistent with the challenge to isolate nuclei from mitotic
196 cells for SN sequencing due to the breakdown of the nuclear envelope during mitosis (**Figure 1G**). Collectively,
197 this comparison underscores the necessity of SN sequencing to representatively capture the gene expression
198 of the STB population in both primary placental tissue and TOs. However, other cell types including mitotic
199 CTB populations (TOs), EVT (tissue), and macrophages (tissue) are enriched in SC and demonstrate a

200 combined SC/SN approach is necessary to capture every cell type in the human placenta or TOs.

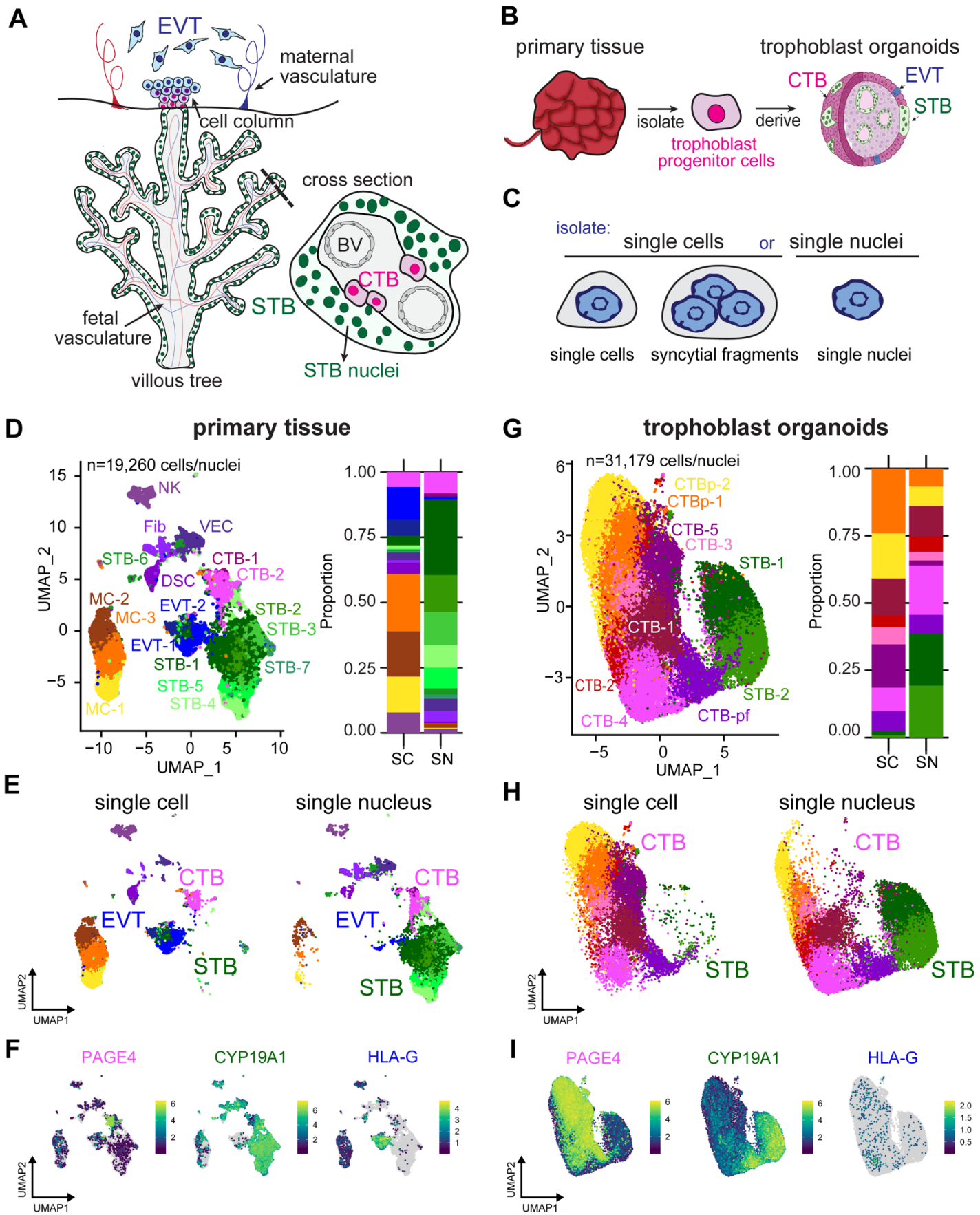

201

Figure 1: Single nucleus sequencing is essential to capture the STB lineage in full-term tissue and TOs. **A** Cartoon of placenta villous tree and cross section, with the multinucleated STB highlighted in green, progenitor CTB cells in magenta, and extravillous cytotrophoblasts in blue. **B** Schematic of organoid generation via isolation of trophoblast progenitor cells from full-term placental tissue. **C** Schematic of experimental setup. Both tissue and TOs were processed into either single cells/syncytial fragments or single nuclei and sequenced. UMAP of integrated SC and SN datasets collected from primary tissue (**D**) and TOs (**G**). Cell/nucleus types are annotated as follows: cytotrophoblast (CTB), cytotrophoblast pre-fusion (CTB-pf), syncytiotrophoblast (STB), extravillous trophoblast (EVT), dendritic stem cell (DSC), vascular endothelial cell (VEC), fibroblasts (Fib), natural killer cell (NK), and macrophage (MC). Cell/nucleus types that contained multiple clusters are identified with -number after the name. **E and H** UMAP of the integrated SC and SN dataset separated into individual UMAPs by single cell or nucleus processing type for primary tissue (E) and TOs (H). **F and I** Expression of key trophoblast markers, including PAGE4 (CTB), CYP19A1 (STB), and HLA-G (EVT) in primary tissue (F) and TOs (I).

Defining trophoblast lineage composition in distinct TO culture conditions

The STB has been historically understudied due to the challenges of its multinucleate architecture. Therefore, we next investigated the impact of TO culture conditions on trophoblast lineage composition using only SN sequencing because it more accurately captured the STB population. To do this, we used TOs isolated from three unique placentas and cultured them each in three distinct culture conditions—standard Matrigel conditions to generate STB^{in} TOs, in suspension to generate STB^{out} TOs, and with NRG1 to enrich for EVT cells (EVT^{enrich}) (**Figure 2A-C, Materials and Methods, Supplemental Table 3-4**). Each organoid condition was processed into suspensions of nuclei, SN sequenced in parallel, and data from each biological replicate integrated, clustered, and plotted on a UMAP. (**Figure 2A-C, Supplementary Figure 2.1A, Supplemental Table 1-2)**. The clusters for each cell type are labeled with numbers assigned in a random order.

We first assessed how CTB subtypes varied amongst the culturing methods that generated different organoid organizations. We found five populations of CTBs that were identified using well-established markers, such as CDH1 and TENM3, and accounted for 53% of the total population in STB^{in}, 38% in STB^{out}, and 57% in EVT^{enrich} (**Figure 2A-C, Supplementary Figure 2.1B**). These CTBs could be delineated into multiple subtypes expressing proliferative markers (KI67 and PCNA in CTB-p), CTB cell column (CTB-CC) markers (LPCAT1, NOTCH1, and ITGA2), or pre-fusion intermediate markers (retroviral fusion protein ERVFRD-1 and GREM2 in CTB-pf) (**Supplementary Figure 2.1B**). STB^{in} and STB^{out} TOs both contained two proliferative CTB populations (CTBp-1 and CTBp-2) that together accounted for 18% of the total nuclear population of each dataset (**Figure 2A-B**). In contrast, there was a single proliferative population in EVT^{enrich} that accounted for 10% of the population, was closer to EVT than CTB on the UMAP, and had downregulated CTB markers and

upregulated EVT markers including HLA-G and MMP2. This suggests that TO-derived differentiated EVTs undergo mitosis, as observed *in vivo* (**Figure 2C, Supplementary Figure 2.1B, D**) (Arutyunyan et al., 2023). In the STB^{in} condition, CTB-2 expressed canonical CTB-CC markers and accounted for 17% of the total nuclear population (**Supplementary Figure 2.1B-C**). The STB^{out} condition predominantly consisted of a single non-proliferative CTB population (CTB-1). A subset of this cluster expressed the CTB-CC marker ITGA2 suggesting this CC population was still present but not identified as a separate cluster (**Supplementary Figure 2.1B-C**). In contrast, three of the five CTB populations in EVT^{enrich} TOs expressed the CTB-CC

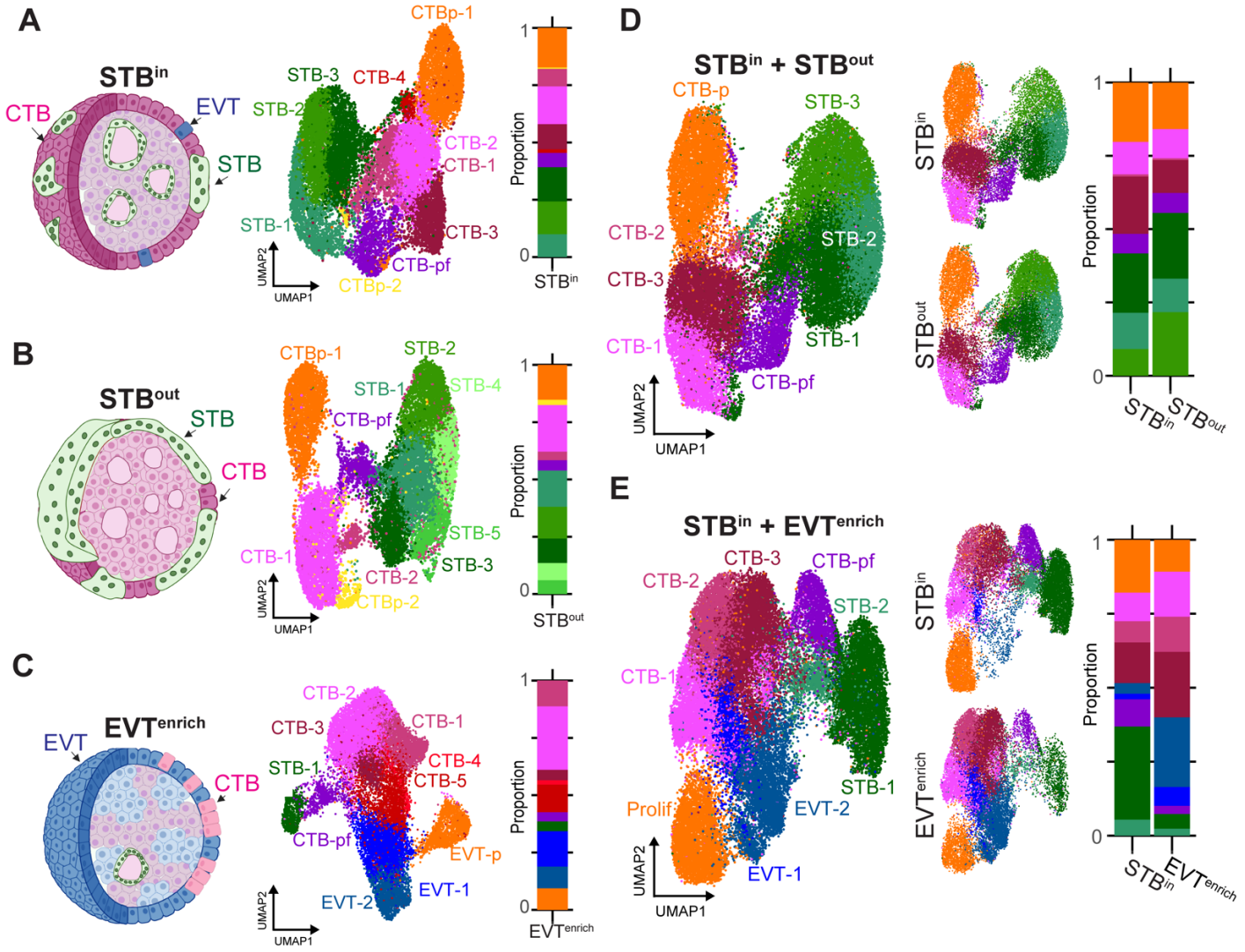

Figure 2: Comparison of TO gene expression in different culture conditions by SN RNA sequencing. TOs were grown with the STB facing inward (STB^{in}), outward (STB^{out}), or induced to differentiate into EVT (EVT^{enrich}). Schematic of TO nucleus type composition (left), UMAP of the individual SN datasets (middle), and barplot showing the proportions of each nucleus type (right) are shown for STB^{in} (**A**), STB^{out} (**B**), or EVT^{enrich} (**C**). UMAP of the integrated datasets (left), integrated dataset split by culture condition (middle), and barplot showing the proportions of each nucleus type (right) are shown for the STB^{in}+STB^{out} integrated dataset (**D**) or STB^{in}+EVT^{enrich} dataset (**E**). Prolif in E refers to proliferative subtype encapsulating both EVT-p and CTB-p.

markers ITGB6 and LPCAT1 (**Supplementary Figure 2.1B-C**), consistent with the function of CTB-CCs to differentiate into EVT (Turco and Moffett, 2019). Finally, CTB-pf accounted for 4% of the total population in STB^{out}/EVT^{enrich} TOs and 6% of STB^{in}, suggesting culture conditions did not dramatically change the proportion of this intermediate cell type (**Figure 2A-C, Supplementary Figure 2.1B**). Thus, while most CTB identities are present across conditions, there are notable differences in the proportion of different CTB subtypes depending on culture conditions.

We next sought to determine how culture conditions influenced the differentiation of CTBs into either the STB or EVTs. In each culture condition STB nuclei were present, accounting for 39% (STB^{in}), 53% (STB^{out}), and 4% (EVT^{enrich}) of the total population (**Figure 2A-C**). As anticipated, few to no EVTs were present in STB^{in} and STB^{out} TOs (**Figure 2A-B)** (Turco et al., 2019; Yang et al., 2023, 2022). In contrast, EVTs accounted for 24% of the total population in EVT^{enrich} TOs and separated into two clusters (EVT-1, EVT-2) (**Figure 2C**). Each had an increased expression of the mature EVT markers HLA-G, MMP2, and DIO2 (**Supplemental Figure 2.1B**). Together, this demonstrates that STB^{out} culture conditions promotes further STB differentiation while EVT^{enrich} conditions promotes EVT differentiation.

To directly compare the relative populations and gene expression between TO culture conditions, we integrated the STB^{in} dataset with either STB^{out} or EVT^{enrich} TOs (**Figure 2D-E**). Each nucleus type retained the expression of canonical markers (**Supplemental Figure 2.2A-B**), but EVT^{enrich} exhibited higher basal expression of the EVT markers HLA-G and DIO2 (**Supplemental Figure 2.2C**). The nucleus types in the STB^{in}+STB^{out} dataset showed significant overlap on the UMAP, indicating relatively consistent gene expression across culture conditions (**Figure 2D**). However, the proportions were not identical for each nucleus type and reflected the differences observed in the individual datasets. Of note, there was a higher percentage of CTB-3 that expressed CTB-CC markers in STB^{in} (20% of STB^{in} and 11% of STB^{out}) and a decrease in the STB-3 population (9% of STB^{in} and 20% of STB^{out}) (**Figure 2D, Supplemental Figure 2.2A**) suggesting that STB^{out} culture conditions promotes STB differentiation and prevents CTB-CC differentiation down the EVT lineage. Despite CTB-pf accounting for 7% of each dataset in STB^{in} and STB^{out}, the STB:CTB ratio was nearly halved in STB^{in} compared to STB^{out} (1.3:1 in STB^{in} versus 2.5:1 in STB^{out}). This indicates a higher proportion of nuclei

278 in STB^{out} TOs have undergone cell-cell fusion to become STB. Similarly, STB^{out} TOs expressed higher levels
279 of key STB markers and hormones, indicating culture in suspension promotes enhanced STB differentiation
280 (**Supplementary Figure 2.2D and Supplementary Figure 3.1D**). These results are consistent with our
281 previous report demonstrating an increase in the number of STB nuclei and enhanced expression of hCG-
282 genes in the STB^{out} condition (Yang et al., 2023). In contrast, the STB^{in}+EVT^{enrich} merged dataset exhibited
283 significantly less overlap on the UMAP and amongst nucleus type proportions (**Figure 2E**). In particular, STB^{in}
284 TOs had a dramatic increase in STB nucleus types (37% of STB^{in} and 7% of EVT^{enrich}) while EVT^{enrich} exhibited
285 an increase in EVT types (5% of STB^{in} and 30% of EVT^{enrich}) (**Figure 2E, Supplemental Figure 2.2B**),
286 validating EVT^{enrich} conditions promote CTB differentiation into EVT instead of STB.

287 Lastly, we compared STB^{out} TOs with a publicly available SN dataset from trophoblast stem cell (TSC)
288 derived STB to identify differences in STB populations that might exist between these models (Wang et al.,
289 2024). We integrated the STB^{out} TO dataset with the TSC dataset, performed clustering, and visualized the
290 results on a UMAP. Both TO and TSC models showed a nearly equivalent composition of trophoblast nucleus
291 types, including CTB-p, CTB-pf, EVTs, and two distinct STB populations (STB-1 and STB-2) (**Supplemental**
292 **Figure 2.3A-C**). Despite similarities in nuclear proportions, pseudobulk differential expression analyses
293 revealed significant differences in the transcriptional profiles of CTB-pf and STB populations derived from TOs
294 and TSCs. TSC-derived CTB-pf and STB clusters highly expressed the EVT marker HLA-G, which was absent
295 in TO-derived CTB-pf and STBs (**Supplemental Figure 2.3D**). Additionally, TO-derived CTB-pf and STBs
296 showed significantly higher expression of STB-associated hormones and other factors, including PSGs, CGBs,
297 CSH1, HOPX, and KISS1 (**Supplemental Figure 2.3D-E**) (Costa, 2016). Therefore, while the two models
298 exhibit a similar proportion of nucleus types, there are notable gene expression differences within each.

299 Together, these data highlight that culture conditions not only influence the composition of trophoblast
300 nucleus types but also drive their differentiation into distinct lineages, consistent with previous reports and
301 underscoring the critical role of the environmental cues present in each culture condition in shaping trophoblast
302 identity (Arutyunyan et al., 2023; Turco and Moffett, 2019; Yang et al., 2023, 2022).

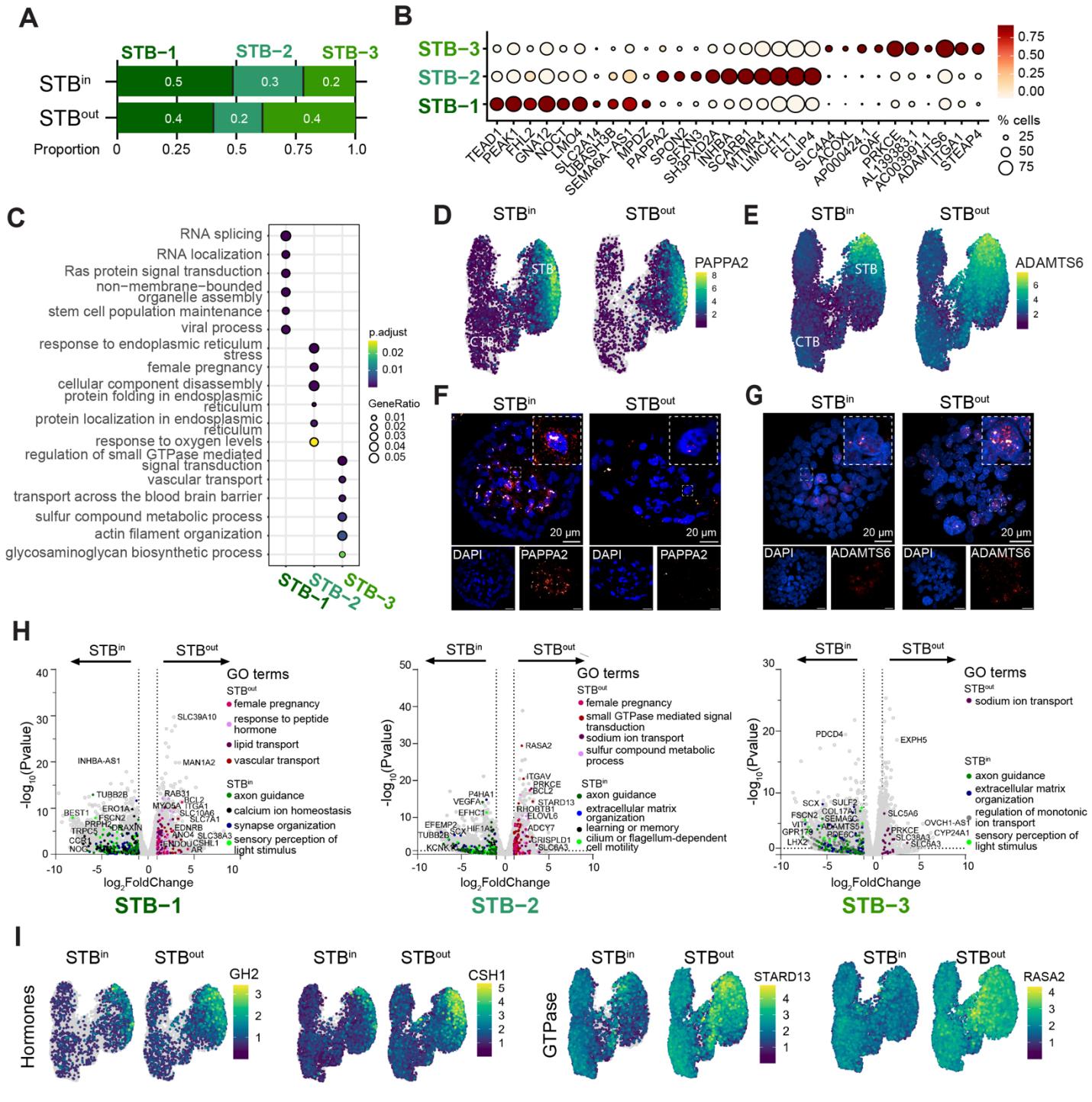

Figure 3: STB subtype analysis and expression differences in STB^{in} vs STB^{out} TOs. A Proportion of each STB subtype in the integrated STB^{in}+STB^{out} dataset. **B** Top differentially expressed genes (DEGs) of each STB subtype is shown as a dot plot. Mean expression is shown as a color scale and percent of nuclei expressing each gene is demonstrated by size of the dot. **C** Top Biological Process GO terms associated with DEGs in each STB subtype was determined with clusterProfiler. **D** Feature Plots of PAPPA2 in STB^{in} and STB^{out} TOs. **E** Feature Plots of ADAMTS6 in STB^{in} and STB^{out} TOs. **F** RNA FISH of PAPPA2 in STB^{in} and STB^{out} TOs. **G** RNA FISH of ADAMTS6 in STB^{in} and STB^{out} TOs. **H** DEseq2 was used to find DEGs between STB^{in} and STB^{out} datasets in STB-1, STB-2, and STB-3 clusters and plotted as a volcano plot. GO terms associated with DEGs in either STB^{in} or STB^{out} were found with clusterProfiler and colored on the UMAP with select representative genes highlighted with text. **I** Feature Plot of representative target genes from E.

314 **Comparative transcriptional profiling reveals three distinct STB subtypes with varied proportions in**
315 **STB^{in} and STB^{out} TOs**

316 Given the increased proportion of STB nuclei in STB^{out} TOs and enhanced expression of typical STB
317 markers in STB^{out} TOs, we next sought to identify the genes that define each STB subtype. To do this, we
318 utilized the merged STB^{in}+STB^{out} dataset that contained three STB subpopulations. This dataset exhibited
319 differential enrichment of each STB subpopulation within the two culture conditions (**Figure 3A**). We first
320 analyzed the genes enriched in each STB subtype and identified hundreds of genes whose expression was
321 conserved in the STB subtypes of both STB^{in} and STB^{out} TOs (**Figure 3B, Supplemental Figure 3.1A,**
322 **Supplemental Table 8**). STB-1 is closest to CTB-pf on the UMAP and expressed many genes previously
323 associated with CTBs, including the transcription factors TEAD1 and TP63 (**Figure 2D, 3B**) (Li et al., 2014;
324 Mizutani et al., 2022). In fact, when the top genes in STB-1 were plotted as a dotplot for every nucleus type in
325 the dataset these genes were most enriched in the CTB subtypes (**Supplemental Figure 3.1B**). The gene
326 ontology (GO) terms associated with STB-1-enriched genes are involved in RNA splicing, stem cell
327 maintenance, and RAS signaling (**Figure 3C, Supplemental Figure 3.1C**). Candidate genes from each of
328 these GO terms demonstrated expression predominantly in CTBs, intermediate expression in STB-1, and lower
329 expression in the remaining two STB populations (**Supplemental Figure 3.1C**). STB-2 expressed a unique
330 subset of genes that included the VEGF receptor FLT1, the TGFβ family member INHBA, and the insulin
331 regulator PAPPA2, associating this subtype with ER stress and oxygen sensing (**Figure 3B-C**) (Barrios et al.,
332 2021; Li et al., 2022; Sasagawa et al., 2021, 2018). Female pregnancy was identified as an enriched GO term
333 in STB-2 (**Figure 3C-D**) and many of the genes found in this term are linked to angiogenesis. This included 8
334 pregnancy specific glycoprotein (PSG) paralogs that are pro-angiogenic, VEGFA, and the growth factor
335 Angiopoietin-2 that facilitates vascular development in specific contexts (Akwii et al 2019, Moore et al 2021)
336 (**Supplemental Table 9**). Interestingly, STB-2 was more abundant in STB^{in} than STB^{out} (**Figure 3A**). We
337 validated this finding with RNA fluorescence in-situ hybridization (FISH) and found an increase in the
338 expression of the STB-2 marker PAPPA2 in STB^{in} TOs compared to STB^{out} (**Figure 3D and F and**
339 **Supplemental Figure 3.3A**). Finally, the top genes in STB-3 included the sodium/bicarbonate transporter
340 SLC4A4, the matrix metalloprotease ADAMTS6, the collagen receptor ITGA1, and protein kinase C epsilon

341 PRKCE (**Figure 3B**) (Cain et al., 2022, 2016; Zeltz and Gullberg, 2016). GO terms demonstrated that the STB-
342 3 cluster was enriched for processes involved in GTPase signaling, vascular transport, and actin organization
343 (**Figure 3C, Supplememtal Figure 3.1C**). Both the vascular transport and transport across the blood brain
344 barrier GO terms were enriched for molecules involved in the transport of small molecules, amino acids, and
345 fatty acids (**Supplemental Table 9**). In contrast to STB-1 and STB-2, the percentage of STB-3 nuclei were
346 doubled from 20% in STB^{in} to 40% in STB^{out}. We validated this finding via RNA-FISH using the STB-3 marker
347 ADAMTS6 and observed increased RNA expression in STB^{out} compared to STB^{in} TOs (**Figure 3E and G and**
348 **Supplemental Figure 3.3B)**. Interestingly, most pregnancy hormones were expressed at similar levels in the
349 STB-2 and STB-3 subtypes but exhibited increased expression in STB^{out} compared to STB^{in} (**Supplemental**
350 **Figure 3.2C-D**). In summary, STB-1 exhibited intermediate gene expression between CTB and STB, STB-2
351 expressed vascular signaling/oxygen sensing factors, while STB-3 was enriched in transport/GTPase signaling
352 functions. Of note, STB-1 and STB-2 nuclear subtypes were enriched in STB^{in} TOs while STB-3 subtype was
353 doubled in STB^{out} TOs, indicating STB nuclear subtype proportions are sensitive to the culture conditions TOs
354 are grown in (**Figure 3A**).

355 Given the different proportions of STB subtypes between STB^{in} and STB^{out} TOs, we next sought to
356 determine if gene expression changed within each STB subtype as a function of culture condition. Therefore,
357 we performed pseudobulk differential expression analysis using DESeq2 to compare gene expression of each
358 STB subtype between STB^{in} and STB^{out} TOs and determined GO terms associated with the differentially
359 expressed genes (DEGs) (**Figure 3H and Supplemental Table 10**) (Love et al., 2014). STB-1 and -2 of STB^{out}
360 TOs were enriched for genes involved in pregnancy including genes in the human placenta lactogen family
361 (CSH1 and CSHL1), growth hormone 2 (GH2), the STB specific gene ENDOU (Haider et al., 2018), and the
362 androgen receptor (AR) (**Figure 3H-I**). In addition, STB in STB^{out} TOs exhibited increased expression of genes
363 involved in GTPase signaling, including the RhoA GAPs STARD13 and GRAF3 (ARHGAP42) (Bai et al., 2013;
364 Ching et al., 2003) (**Figure 3H-I**). All three STB subtypes in STB^{out} TOs exhibited an enrichment in transport-
365 associated proteins, consistent with the STB being proximal to media (**Figure 3H, Supplemental Figure 3.1E**).
366 In contrast, STB^{in} TOs were enriched in extracellular matrix organization genes but their expression was not
367 specific to STB subtypes (**Figure 3H and Supplementary Figure 3.1F**). The STB-2 subtype in STB^{in} TOs had

368 increased expression of the hypoxia associated genes LIMD1, HILPDA, and HIF1A as well as the
369 angiogenesis-associated proteins VEGFA and FLT1 (**Figure 3H, Supplemental Figure 3.1G**) (Foxler et al.,
370 2018; Rodriguez and Kersten, 2020; Shibuya, 2011), consistent with the increased proportion of the oxygen
371 sensing STB-2 subtype in STB^{in}. Together, these results demonstrate that there are at least three
372 subpopulations of STB in trophoblast organoids, which differ both in their relative proportions and transcriptional
373 signature between culture conditions.
374

375 **Pseudotime and gene network analysis reveals gene regulators in STB^{out} TOs, including the chromatin**
376 **remodeler RYBP**

377 To assess whether distinct nuclear subtypes represented a STB differentiation trajectory in TOs, we next
378 performed pseudotime gene expression inference using the integrated STB^{in} and STB^{out} datasets described
379 above (**Figure 2D**). We utilized the Slingshot algorithm to establish the global lineage structure for each dataset
380 using undefined starting and ending clusters (Street et al., 2018). Following this, we depicted the pseudotime
381 progression on the UMAP plot for the STB lineage (**Figure 4A**). This visualization revealed a continuous
382 trajectory starting from CTB-p subtype, traversing through CTBs to CTB-pf, and progressing through STB-1
383 and STB-2 before culminating in the STB-3 subtype (**Figure 4A**). To find genes associated with pseudotime,
384 we performed an association test with tradeSeq and found that STB differentiation was marked by an increase
385 in well-known STB marker genes, including ADAM12, PLAC4, and PSG6 (**Figure 4B**) (Aghababaei et al., 2015;
386 Chen et al., 2022; Moore et al., 2021; Tuohey et al., 2013). Next, we conducted a comparative pseudotime
387 expression analysis between STB^{in} and STB^{out} conditions. Our findings revealed enrichment of several STB-
388 associated genes in STB^{out}, such as the secreted metallopeptidase protein ADAM12, the progesterone
389 synthesis enzyme CYP11A1, and the proteoglycan synthesis gene MAN1A2 (**Figure 4C**) (Aghababaei et al.,
390 2015; Zhu et al., 2023). Interestingly, the chromatin remodeler RYBP and transcriptional activator AFF1 were
391 two genes most significantly associated with the CTB to STB pseudotime trajectory and enhanced in STB^{out}
392 TOs (Figure 4B-C), suggesting they may play roles in initiating transcription of genes involved in STB^{out} nuclear
393 differentiation.

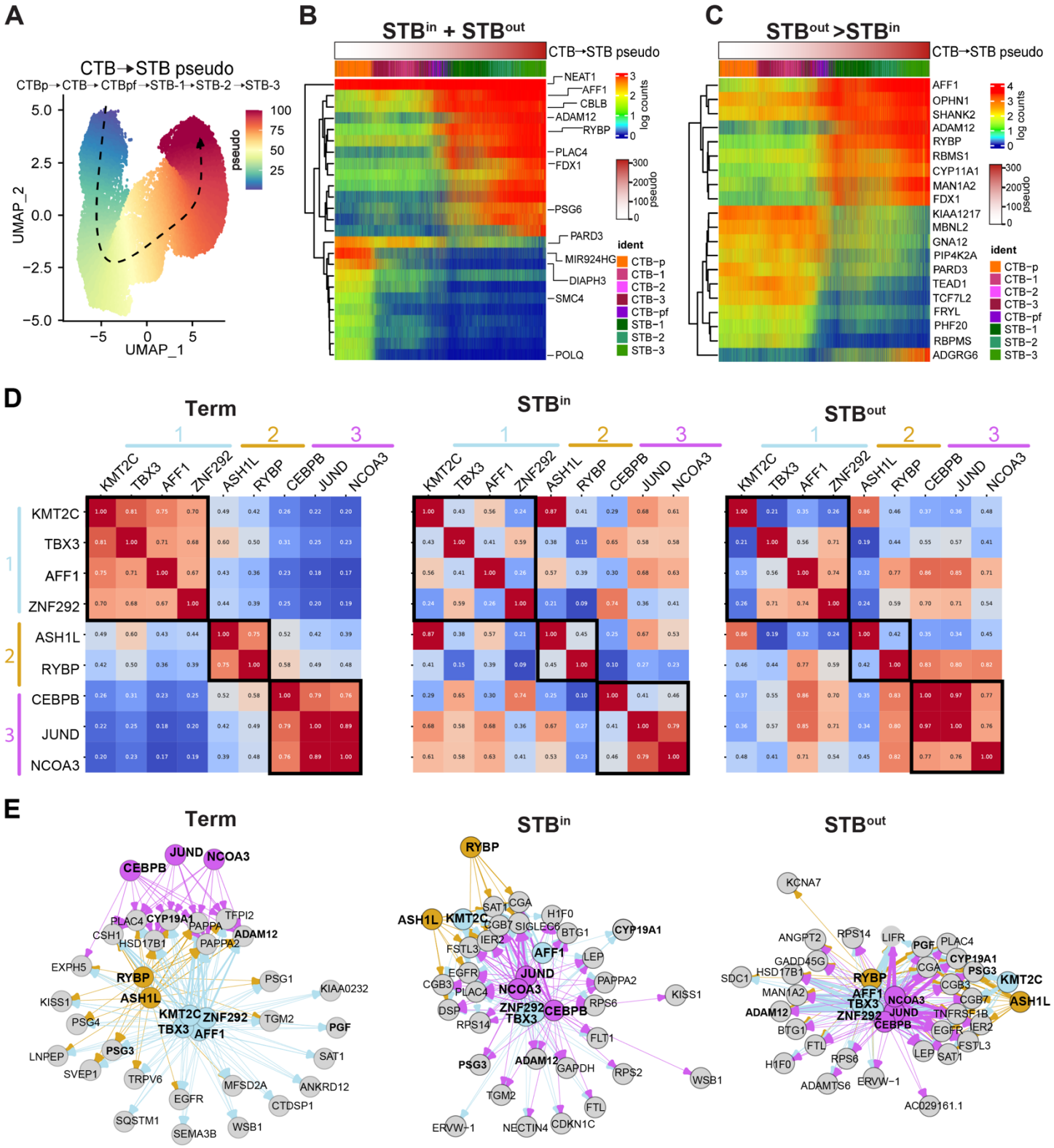

Figure 4: Trajectory and gene regulatory network analysis reveals transcription factors and chromatin remodelers associated with STB differentiation. **A** Pseudotime was performed with Slingshot and assigned pseudotime value for each nucleus type is overlayed as a color scale on the UMAP from time 0 (blue) to time 100 (red). Arrow demonstrates directionality of the trajectory. Top genes associated with pseudotime (**B**) or enriched in STB^{out} compared to STB^{in} (**C**) are plotted on a barplot with nuclei ordered with the pseudotime seen in A. Logcounts and pseudotime are demonstrated as a color scale bar and the identity of each nucleus is

labeled with a color as indicated in the legend. **D** TF/CR and TG pairs were identified via Velorama and plotted as a similarity matrix to show the overlap in TGs for each TF/CR. Each module discussed in the text is labeled as 1, 2, or 3 and colored with blue, orange, or pink respectively. **E** Network graphs of TF/CRs and their respective TGs were plotted with igraph. Each TF/CR and respective arrows were false colored as per the module labels in D. Grey circles represent the target genes. Target genes that are shared among all three sample types are bolded. The width of the arrow from each TF/CR to each TG represents the interaction strength score determined with Velorama and the color of the arrow represents the module from which the interaction arises.

To obtain a global view of candidate transcription factors and chromatin remodelers involved in STB differentiation in tissue, STB^{in}, and STB^{out} TOs we next turned to a gene network analysis approach. We isolated the subset of nucleus types involved in STB differentiation (CTB, CTB-pf, and STBs) from each dataset and performed RNA velocity using spliced/unspliced matrices and plotted trajectories from each on a UMAP integrated for replicates of each sample type. This analysis creates a trajectory like slingshot but instead of accounting for pseudotime with bulk RNA expression, it leverages transcript splicing dynamics (Manno et al., 2018). The predominance of STB nuclei in the SN full-term tissue dataset precluded the ability to attain sufficient CTB-pf nuclei, but the velocity map demonstrated CTB differentiating into two STB lineages (**Supplemental Figure 4.1, full-term**). Given the decreased STB:CTB ratios present in organoids, we were able to capture high numbers of CTB-pf nuclei and observed that this population is a precursor to the STB, as anticipated (**Supplemental Figure 4.1, STB^{in} and STB^{out}**). We then employed Velorama to infer gene regulation in these cells. Velorama is an RNA Velocity-based causal inference method that accounts for the multi-trajectory development of cellular state. It infers temporal causality on a directed acyclic graph where each node is a cell, and the edges indicate the velocity-implied direction of differentiation. Velorama derives gene regulatory networks by training a neural network to predict target gene expression profiles given regulator genes, such as transcription factors (TFs), and outputs an interaction score for every TF and target gene (TG) combination (Singh et al., 2024). Given the identification of the chromatin remodeler RYBP in the Slingshot analysis, we expanded Velorama to include other known chromatin remodelers (CRs), as they also have the potential to regulate gene expression levels.

To dissect the functional interactions between TF/CRs, we first compared the similarity of TGs interacting with each TF/CR and plotted this as a heatmap with a score of 1 indicating all TGs are shared and a score of 0 indicating no overlap (heatmap demonstrates high overlap in red and low overlap in blue, **Figure**

433 **4D**). In full-term tissue, these TF/CR fell into three modules that shared most target genes: 1-
434 KMT2C/TBX3/AFF1/ZNF292 (blue), 2-ASH1L/RYBP (orange), and 3-CEBPB/JUND/NCOA3 (pink) (**Figure**
435 **4D**). In contrast to full-term tissue, most TGs in STB^{in} organoids were associated with
436 AFF1/JUND/NOCA3/ZNF292/TBX3/CEBPB in no module order (**Figure 4D**). Finally, STB^{out} appeared to have
437 a similar distribution of TF/CRs as STB^{in}, apart from an increased prevalence of RYBP association with target
438 genes in STB^{out} (**Figure 4D**).

439 We next evaluated the specific TGs in each condition to predict the possible functions of the TF/CR and
440 TG pairs. In full-term tissue, many STB-specific target genes were found to be associated using RNA velocity
441 including CYP19A1, MFSD2A, ADAM12, PSGs, human placenta lactogen (CSH1), and the placenta specific
442 insulin regulator PAPPA enriched in STB of full-term tissue (Wang et al., 2024). Module 3 was only associated
443 with a handful of genes at full-term and with low interaction scores (interaction score demonstrated by arrow
444 width). In contrast, Module 3 had a much stronger prevalence in both the number of target genes and interaction
445 scores in both STB^{in} and STB^{out} organoids with some similar genes (conserved genes bolded, ADAM12,
446 CYP19A1, PGF, PSG3) and some unique to organoids, particularly of note being hCG genes (CGA, CGB4,
447 CGB7) (**Figure 4E**), whose expression is known to be decreased in the STB of full-term tissue (Rull and Laan,
448 2005). STB^{in} was the only condition to show a link between the TF/CRs and the VEGF receptor FLT1, consistent
449 with the enrichment of hypoxic/angiogenic associated genes in the STB-2 subtype of STB^{in} compared to STB^{out}
450 (**Figure 3H, 4D**). Importantly, this analysis independently identified both RYBP and AFF1 as transcription
451 effectors involved in the expression of STB TGs, consistent with our pseudotime analysis (**Figure 4A-C**). AFF1
452 was associated with most TGs in all three sample types (**Figure 4E**). In contrast, while RYBP was associated
453 with most STB marker genes in full-term tissue and STB^{out}, it was associated with only a few TGs in STB^{in}
454 (**Figure 4E**). In fact, RYBP was associated with genes that were enriched in STB^{out} organoids in the Slingshot
455 analysis (ADAM12 and MAN1A2) but not in STB^{in} TOs (**Figure 4B-E**), supporting the hypothesis that RYBP
456 could be a modulator of a specific lineage of STB nuclear subtype differentiation. In summary, this gene network
457 analysis suggests that many TF/CR and TG interactions are shared amongst tissue and TOs. However, many
458 interactions in TOs also change as a function of culture condition. While module 3 is most linked to TGs
459 expressed in TOs, RYBP is linked specifically to TGs expressed in tissue and STB^{out} TOs, but not STB^{in} TOs.

460 **RYBP is a STB-specific nuclear marker involved in silencing gene expression characteristic of the STB-**
461 **2 nuclear subtype**

462 To validate the analyses described above, we selected RYBP as a model target gene for its potential
463 role in STB nuclear subtype differentiation and based on the availability of well-validated antibody reagents.
464 RYBP contains chromatin remodeling activity as part of the PRC1 histone ubiquitination complex and can both
465 increase and decrease the transcription of target genes (Rose et al., 2016; Silva et al., 2018). The expression
466 dynamics of RYBP was directly correlated with the differentiation trajectory from CTB to STB, with upregulated
467 expression beginning in CTB-pf (**Figure 4B**). We first visualized RYBP in full-term tissue sections, using E-
468 cadherin as a marker of CTB and Cytokeratin-7 as a marker of CTB and STB cells. STB can be clearly
469 designated as regions expressing Cytokeratin-7 but not expressing E-Cadherin, as validated with the STB-
470 specific marker ENDOU (**Supplementary Figure 5.1**). We found that RYBP exhibited STB-specific localization
471 in term placenta tissue (**Figure 5A**). To confirm this result in TOs, we visualized RYBP at the protein level in
472 each sample type with immunofluoresence (IF) using E-cadherin as a CTB marker and CGBs as STB specific
473 markers (**Figure 5B-C**). RYBP exhibited STB specific expression in both STB^{in} and STB^{out} TOs. Together this
474 suggests that RYBP is a novel marker of STB nuclei in tissue and TOs. We hypothesized that RYBP could play
475 a role in guiding STB nuclei toward a specific nuclear subtype during differentiation. To test this, we performed
476 gene editing in TOs with CRISPR/Cas9 to delete RYBP and confirmed this knock-out by sequencing and IF
477 (**Figure 5D** and **Supplemental Figure 5.2A**). In parallel, we generated TOs with AFF1 deletion, as it was also
478 associated with the STB differentiation trajectory and confirmed the knockout by sequencing (**Figure 4** and
479 **Supplemental Figure 5.2B**). However, despite testing several antibodies, none were suitable for IF localization
480 of AFF1. We generated three homozygous knockouts clones of each line ($RYBP^{-/-}$) or AFF1 ($^{-/-}$) and compared
481 their morphologies to three control TO lines that contained the Cas9 plasmid but a scrambled gRNA (WT). No
482 difference in the overall morphology of TOs was found, and size and number of nuclei within the STB remained
483 constant (**Figure 5D**). To determine if gene expression differences were found in the TOs lacking RYBP or
484 AFF1, we performed bulk RNA sequencing of each RYBP($^{-/-}$), AFF1 ($^{-/-}$) or WT lines in STB^{in} TOs. We found
485 that deletion of either RYBP or AFF1 resulted in significant increased expression of genes associated with the
486 STB-2 oxygen sensing subtype, including FLT1, PAPPA2, SPON2, SFXN3, and many of the PSG hormones

involved in angiogenesis (**Figure 5E**, **Supplemental Figure 5.3, Supplemental Table 11**). RYBP($^{-/-}$) TOs upregulated transcripts that were not expressed in WT TOs or AFF1$^{-/-}$TOs (**Figure 5E and Supplemental Figure 5.3**). RYBP is a component of a non-canonical Polycomb complex that transcriptionally silences genes (Rose et al., 2016). In addition to the upregulation of the STB-2 genes, its knockout led to the upregulation of many genes not typically expressed in TOs including COL18A1, SEMA5A, CARD11, and MSX1, likely due to the loss of this silencing function (**Figure 5E**).In contrast, the human placenta lactogen gene (CSH1) was significantly upregulated in WT TOs compared to RYBP$^{-/-}$ and AFF1$^{-/-}$ TOs, suggesting deletion of both RYBP and AFF1 affect the expression of a hormone increased in STB^{out} TOs (**Figure 5E, Supplemental Figure 5.3,**

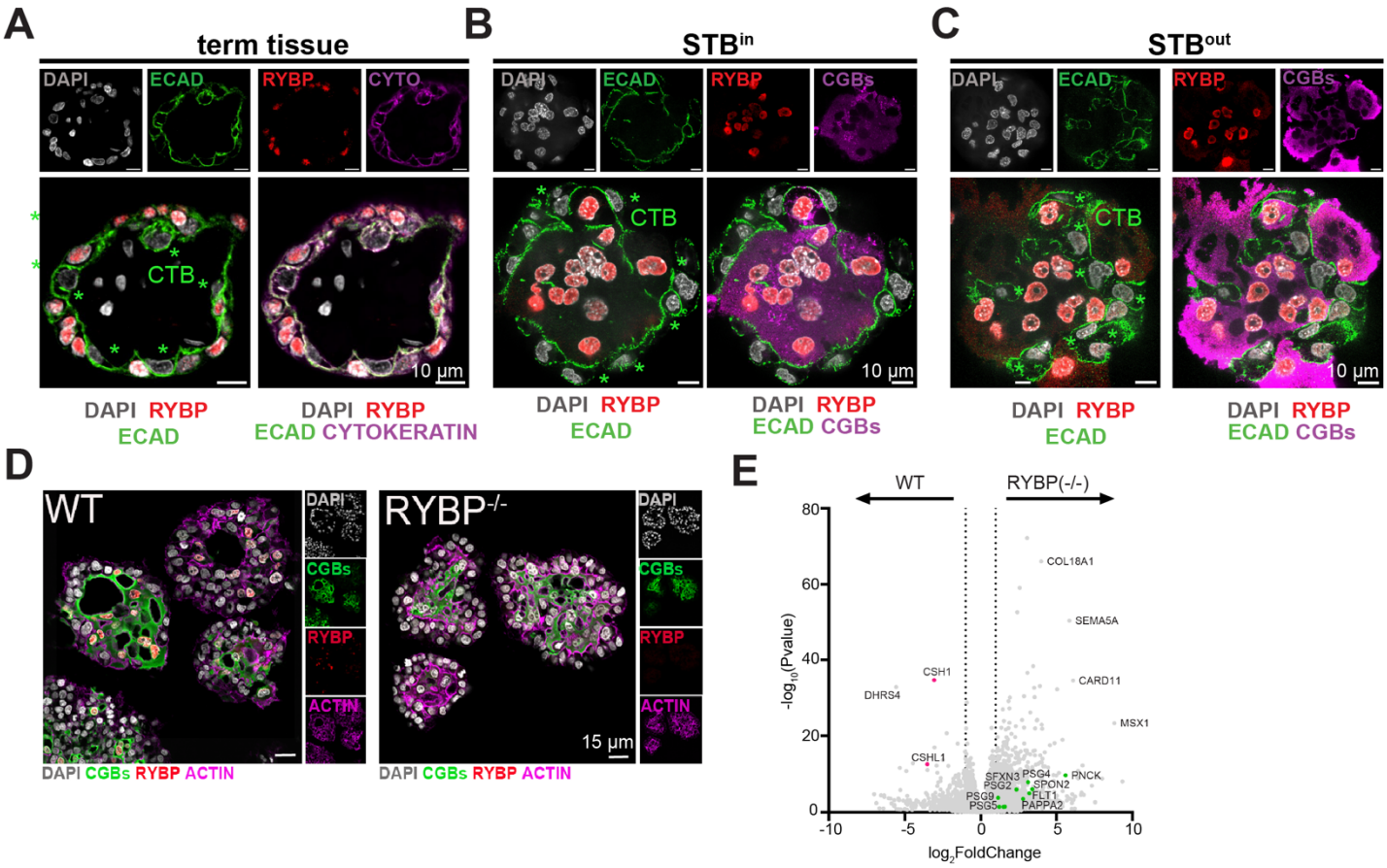

Figure 5 RYBP is a marker of STB and its deletion downregulates STB-2 marker genes. A Immunofluorescence of full-term tissue was performed with E-cadherin (ECAD), cytokeratin (CYTO), and RYBP and stained with DAPI to label nuclei. Immunofluorescence of STB^{in} TOs (**B**) or STB^{out} TOs (**C**) was performed with chorionic gonadotropin (CGBs) to label STB, RYBP, and E-cadherin (ECAD) to mark cell boundaries. TOs were further stained with DAPI to label nuclei. Green stars represent CTB cells, as marked by E-cadherin, and are negative for RYBP. **D** Immunofluorescence of WT or RYBP-/- STB^{in} TOs performed with RYBP and CGBs and stained with DAPI and Actin. **E** Bulk RNA sequencing of WT or RYBP(-/-) STB^{in} TOs was performed and analyzed with DESeq2 to determine differential gene expression. Dotted line represents a $\log_2$ fold change greater than 1. Genes enriched in the STB-2 subtype are labeled in green.

and Supplemental Table 11). However, no further STB-3 subtype genes were found to be upregulated compared to control in the STB^{in} TOs tested. Together, these results validate the predictions from the trajectory analyses described above and suggest that AFF1 and RYBP act to silence the STB-2 nuclear subtype and activate human placenta lactogen in TOs.

Comparison of STB differentiation in TOs to first trimester and full-term placental tissue

Having identified several differences in STB differentiation between STB^{in} and STB^{out} TOs, we next sought to identify how these differences relate to placenta tissue across gestation. We used a publicly available first trimester SN sequencing dataset and integrated this data with the full-term tissue and TOs described above (**Supplemental Figure 6.1A**). Because tissue-derived datasets contain a large proportion of non-trophoblast

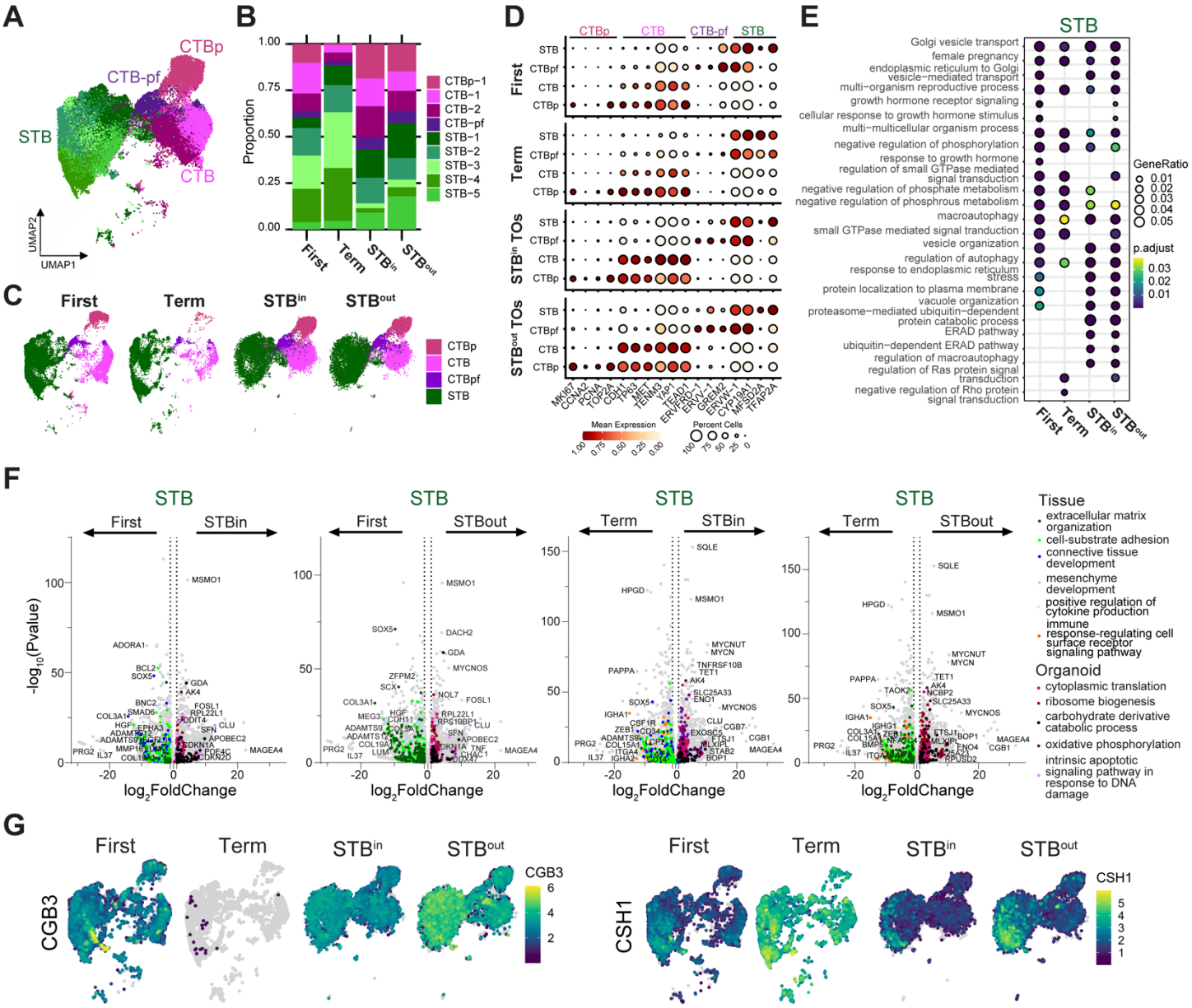

515 **Figure 6: Similarities and differences between STB in first trimester and full-term tissue and TOs. A**
516 UMAP of the integrated SN dataset including first trimester, full-term tissue, STB^{in} TOs, and STB^{out} TOs. **B**
517 Relative proportion of each nucleus type for each sample in the integrated dataset in A. **C** UMAP of the
518 integrated dataset split by sample type. The five STB subtypes were merged into a single STB subtype while
519 the two non-proliferative CTB subtypes were merged. **D** Dot plot of key trophoblast marker genes in the STB
520 lineage with heatmap representing mean gene expression and size of the dot representing the percent of nuclei
521 expressing each marker. The labels on the top of the graph refer to the established marker genes used to
522 identify the identity of each cluster. **E** The top DEG in the STB of each sample type were analyzed for biological
523 process GO term enrichment with clusterProfiler and plotted as a dotplot. **F** DEseq2 was used to find DEGs
524 between different sample types for the merged STB cluster. GO terms for DEGs enriched in each sample type
525 were found with ClusterProfiler and colored on the UMAP with select representative genes highlighted in text.
526 **G** Feature plots demonstrating RNA expression of selected genes.
527
528
529 nucleus types, we subset the integrated dataset to contain only trophoblasts in the STB lineage, which included
530 both proliferating CTBs (CTB-p), CTBs (CTB-1 and CTB-2), pre-fusion CTBs (CTB-pf), and five distinct STB
531 populations (**Figure 6A-6B**, **Supplemental Figure 6.1A-D**). The proportion of STB:CTB was higher in full-term
532 tissue than in first trimester tissue (7:1 at full-term vs 1.5:1 in first trimester, combined dataset), as anticipated
533 given the higher proportion of CTBs in first trimester (**Figure 6B**) (Benirschke et al., 2012; Mayhew, 2014). Of
534 note, the STB:CTB ratios in TOs more closely resembled first trimester than term tissue in both culture
535 conditions (1:1 for STB^{out} and 0.6:1 for STB^{in}) (**Figure 6B**). The tissue and TO samples exhibited dramatically
536 different proportions of each CTB (CTB-1-2) subtype and each STB (STB1-5) subtype, which indicates sample
537 to sample heterogeneity (**Figure 6A-B, Supplemental Figure 6.1A-C**). Therefore, we merged the two CTB
538 and five STB populations together to globally detect the conserved and differentially expressed genes among
539 the STB or CTB populations (**Figure 6C**). We first analyzed the expression of canonical marker genes for each
540 nucleus type (for example TP63/TENM3 in CTB and CYP19A1 /TFAP2A in the STB) and found that each
541 sample expressed these markers (**Figure 6D**), suggesting general conservation across both tissue types and
542 TO conditions. To dissect what was different amongst the samples, we next analyzed the enriched genes in
543 each nucleus type and identified GO terms associated with these genes for each sample type (**Figure 6E and**
544 **Supplemental Figure 6.1E and Supplemental Table 12 and 13**). GO terms associated with the CTB
545 populations were remarkably conserved amongst all sample types (**Supplemental Figure 6E**). In contrast,
546 STB exhibited greater diversity of functions between sample types (**Figure 6E**). While GO terms involved in
547 ER to Golgi transport and hormone production were conserved in all STB samples, many processes were
548 found only within a subset of sample types (**Figure 6E**). For example, genes with ER stress, ER associated

549 degradation, and macroautophagy GO terms were expressed in TOs but not in tissue. In contrast, GTPase
550 signaling and vesicle organization were present in first trimester, term, and STB^{out} TOs, but not in STB^{in} (**Figure**
551 **6E**). Together, these findings suggest that the STB exhibits greater heterogeneity in function across sample
552 types than do CTBs.

553 To determine what genes were significantly different in each sample, we performed pseudobulk
554 analyses using DESeq2, plotted genes on a Volcano plot, and colored genes significantly associated with
555 different GO terms (**Figure 6F and Supplemental Table 14**). We performed this analysis comparing STB in
556 either first trimester tissue to TOs (STB^{out} or STB^{in}) or full-term tissue to TOs (STB^{out} or STB^{in}) (**Figure 6F**).
557 Many GO terms were enriched across all comparisons. This included an increase in extracellular matrix, cell
558 substrate adhesion, and connective tissue development genes within the tissue datasets, with a particular
559 enrichment of collagen genes and matrix metalloproteases (ADAM and MMP family members) (**Figure 6F**) (Qu
560 and Khalil, 2022). In contrast, the STB present in organoids exhibited an enrichment of genes involved in
561 cytoplasmic translation/ ribosome biogenesis as well as oxidative phosphorylation/ DNA damage (**Figure 6F**).
562 In addition, genes associated with cytokine production and the immune response based on GO terms were
563 present in full-term tissue but not first trimester tissue or TOs (**Figure 6F**). Therefore, while STB of TOs and
564 tissue share many conserved marker genes, a subset of STB gene expression is differentially regulated
565 between tissue and TOs.

566 We next evaluated the expression of genes known to change throughout gestation in each sample type.
567 For example, many hormones are differentially released throughout pregnancy with first trimester tissue
568 exhibiting high hCG production (CGB genes) and full-term tissue releasing more human placenta lactogen
569 (CSH genes) (Costa, 2016; Rull and Laan, 2005; SAMAAN et al., 1966). Consistent with these gestational
570 hormone trends, STB from first trimester expressed hCG genes while there was no expression in full-term
571 tissue (**Figure 6G, Supplemental Figure 6.1F**). Further, full-term tissue exhibited an increase in CSH1
572 expression compared to first trimester (**Figure 6G, Supplemental Figure 6.1F**). STB^{in} and STB^{out} TOs
573 expressed both hormones in the STB suggesting organoids can produce hormones differentially expressed
574 throughout gestation (**Figure 6G, Supplemental Figure 6.1F**). STB^{out} TOs exhibited an increase in expression
575 of both hormones compared to STB^{in} TOs (**Figure 6G, Supplemental Figure 6.1F**). Consistent with previous

576 reports, there was an increase in the expression of FLT1 and decrease in PAPPA in the STB of first trimester
577 compared to full-term tissue, with TOs resembling first trimester expression (**Supplemental Figure 6.1G-H)**
578 (Wang et al., 2024). Together, these results demonstrate that while the STB of each sample expresses key
579 STB marker genes, both gestational age and trophoblast organoid culture conditions can modify the gene
580 expression patterns of the STB.
581
582 **Discussion**
583 A critical barrier to understanding human gestation has been the limited number of accessible models
584 for the placenta. In this study, we conducted comparative SC and SN RNA sequencing on full-term placenta
585 tissue and TOs. Our findings demonstrate that SN sequencing is crucial for capturing the STB lineage due to
586 its distinct syncytial structure. In contrast, SC sequencing enriched for mitotic cell populations in TOs and EVT
587 in tissue, suggesting the isolation approach chosen depends on your trophoblast cell type of interest. We
588 characterized the nucleus types in each TO model and utilized DEG and pseudotime analyses to define three
589 STB subtypes present in both STB^{in} and STB^{out} TOs, albeit at different ratios. These include a juvenile
590 population that exhibited intermediate CTB and STB expression (STB-1), an FLT1+ population enriched in
591 genes involved in oxygen sensing and the stress response (STB-2), and a final subtype enriched in transport
592 and GTPase signaling molecules (STB-3). We identified the chromatin remodeler RYBP as a gene linked to
593 STB differentiation. We validated that RYBP exhibits STB specific expression in TOs and tissue via
594 immunofluorescence and utilized CRISPR to knock out RYBP in TOs. Deletion of RYBP in TOs upregulated
595 genes that define the STB-2 subtype and downregulated the placenta hormone human placenta lactogen.
596 Finally, we compared STB gene expression between placental tissues from first trimester and full-term to TOs.
597 This showed that although standard STB differentiation markers are maintained in all, there is substantial
598 heterogeneity in STB gene expression between the different sample types. Together, these results draw
599 important implications for our understanding of STB nuclear differentiation and show how TOs can serve as
600 relevant STB models.
601 STB^{out} TOs grown in suspension maintain native polarity and exhibit an increase in syncytia size, with
602 >50 nuclei/syncytia in STB^{out} compared to ~10 nuclei/syncytia under standard STB^{in} culture conditions (Yang
603 et al., 2023). However, it was unknown whether CTB grown via this method maintained their proliferative

604 capacity. Here we show that the proportion of mitotic cells remains constant between TOs grown in STB^{in} and
605 STB^{out} conditions, suggesting culture in suspension is not a terminal, post-mitotic state. In fact, the proportion
606 of STB nuclei increased in the STB^{out} condition was concurrent with a decrease in the CTB-CC population. *In*
607 *vivo*, CTB-CC cells sit adjacent to the villous trees and maternal uterus and are thought to progressively
608 differentiate into EVT cells that then can invade into the uterus (Arutyunyan et al., 2023; Boyd and Hamilton,
609 1970; Turco and Moffett, 2019). Therefore, the increase of STB in the STB^{out} condition could be caused by
610 promotion of STB lineage and an inhibition of differentiation down a CTB-CC or EVT lineage.

611 The enrichment of STB nuclei in SN sequencing allowed us to identify and define three populations of
612 STB in the STB^{in} and STB^{out} TO conditions. STB-1 represented a juvenile population undergoing a transition
613 from CTB to STB gene expression. These nuclei may have recently incorporated into the syncytia and are
614 actively undergoing differentiation at the time of sequencing. STB-2 expressed the VEGF receptor FLT1 and
615 is enriched in genes involved in responding to oxygen levels and ER stress, suggesting STB-2 might play a
616 role in responding to low oxygen levels. Finally, STB-3 exhibits an increase in GTPase signaling molecules and
617 transporter proteins. Importantly, culture conditions changed the relative enrichment of these subtypes.
618 Whereas STB^{in} TOs were enriched for the juvenile STB-1 and oxygen sensing STB-2 populations, STB^{out} TOs
619 exhibited an increase in the transport/GTPase STB-3 subtype. We hypothesize the STB-3 subtype is a terminal
620 differentiation state as it appears at the end of the slingshot pseudotime trajectory. In fact, in addition to
621 exhibiting a higher proportion of the STB-3 subtype, STB^{out} TOs express higher concentrations of key STB
622 pregnancy hormones in all nuclear subtypes suggesting culturing in suspension may promote terminal STB
623 differentiation. An alternative hypothesis, however, is that nuclei in STB^{in} and STB^{out} TOs exhibit distinct
624 lineages trajectories. Testing these hypotheses will require future experiments tracing nuclear subtypes through
625 time.

626 Why might changing culture conditions influence the distribution and gene expression of STB nuclear
627 subtypes? We hypothesize growth in either extracellular matrix (STB^{in}) or suspension (STB^{out}) impacts both the
628 cell orientation and environmental cues each cell type is exposed to like oxygen concentrations, cell and
629 membrane tension, and media flow dynamics. Future studies dissecting each environmental cue and the
630 differentiation of STB nuclei through time and space will help elucidate the molecular mechanism driving each

631 STB subtype. Of note, these three STB subtypes are remarkably like those recently defined in first trimester
632 and full-term tissue: a juvenile population, a FLT1 expressing population enriched in genes involved in oxygen
633 sensing, and a PAPPA positive population that expresses GTPase signaling molecules and hormones (Wang
634 et al., 2024). The distribution of STB subtypes defined in Wang et al (2024) also changed throughout gestation
635 with the oxygen sensing STB nuclear subtype increased in the first trimester and the GTPase/hormone subtype
636 increased at term and implies the environmental cues the STB experiences throughout gestation may affect
637 STB subtype distribution *in vivo* similar to what is seen in TOs. This resemblance suggests TOs can recapitulate
638 similar nucleus subtypes as those seen *in vivo*, indicating their strength as an experimental model and
639 highlights the importance of dissecting the environmental cues that contribute to each STB subtype *in vitro.*

640 How might these distinct nuclear transcriptional identities affect the function of the STB? Despite the
641 STB being one large cytoplasm where molecules can freely mix by diffusion, it has long been suggested to
642 contain distinct cytoplasmic zones that specialize in different functions (Benirschke et al., 2012; Burgos and
643 Rodríguez, 1966; Burton, 1990). For example, STB cytoplasmic regions adjacent to the fetal vasculature
644 dramatically thin presumably to facilitate diffusional exchange of gas and nutrients and express angiogenic
645 promoting proteins. In contrast, regions where hormones are produced have dense packing of membraneous
646 organelles and express protein trafficking molecules (Baczyk et al., 2004; Beck et al., 1986; Burton and
647 Jauniaux, 1995; Clark et al., 1998; Hempstock et al., 2003; Jauniaux et al., 2003; Khaliq et al., 2009; Morrish
648 and Marusyk, 1997; Mouzon, 1997; Sharkey et al., 1993). One potential mechanism for creating these distinct
649 cytoplasmic zones is nuclear specialization, whereby individual nucleus identities might be spatially localized
650 to different cytoplasmic regions, as has been demonstrated for nuclei in syncytial muscle fibers (Kim et al.,
651 2020, Petrany et al., 2020). Different nuclear identities likely arise from a combination of differentiation
652 pathways and environmental cues. The generation of an organoid cell culture model that recapitulates the STB
653 nuclear identities seen *in vivo* is a critical advancement towards deciphering the mechanisms that allow the
654 giant STB cell to effectively carry out its many essential functions.

655 To dissect the transcription factors that drive STB differentiation we applied gene regulatory analysis
656 and identified multiple TF/CR modules potentially involved in differentiation of STB in full-term tissue and TOs.
657 Interestingly, the module most associated with STB^{in} included the TF CEBPB, which is important for placenta

658 development in mice and was recently found to be involved in STB differentiation in first trimester but not in
659 full-term tissue (Bégay et al., 2004; Wang et al., 2024). Consistent with these results, we found that the TF
660 CEBPB was only associated with a few genes in our independent full-term tissue dataset, suggesting that STB
661 of TOs might employ transcriptional programs characteristic of the first trimester. The final module includes the
662 CR RYBP, which is involved in a non-canonical form of the PRC1 polycomb complex that ubiquitinylates
663 histones and can modulate gene expression (Rose et al., 2016; Silva et al., 2018). We demonstrate that RYBP
664 exhibits STB-specific expression in TOs and tissue. We predicted that RYBP might mediate the differentiation
665 of STB nuclei into specifc nuclear subtypes. To test this idea, we deleted RYBP with CRISPR/Cas9 in TOs
666 and observed an increase in many STB-2 nuclear subtype marker genes and a significant decrease in the
667 human placenta lactogen gene. This suggests that RYBP acts to downregulate the STB-2 nuclear subtype in
668 STB^{in} TOs. Future work delving into the exact distribution of STB nuclear subtypes in STB^{in} and STB^{out} TOs
669 will enable us to dissect if RYBP also plays a role in activating the STB-3 subtype, or simply inhibiting the STB-
670 2 subtype. Of note, RYBP deletion in mice is embryonic lethal due in part to a failure to form trophectoderm
671 and subsequent invasion defects (Pirity et al., 2005), consistent with a possible role of RYBP on STB
672 differentiation in human placenta.

673 While the global subtypes found in first trimester, full-term tissue, STB^{in} TOs, and STB^{out} TOs were
674 similar, many genes were differentially expressed in each STB population. One significant difference between
675 the STB of full-term tissue and TOs was in hormone expression. It has long been appreciated that the STB
676 differentially expresses hormones as a function of gestational age (Costa, 2016; Kumar and Magon, 2012), but
677 it was not known 1- how TOs mirror this expression and 2- how isolation of TOs from different stages of tissue
678 gestation affected expression. We found that while the TOs used in this study were derived from full-term CTBs,
679 the STB associated with these organoids express hormone transcripts classically associated with early
680 gestation. This suggests that the cues that restrict these hormones to different gestational stages *in vivo* are
681 not intrinsic to the isolated CTBs and can be studied in full-term derived TOs. Future work adding maternal
682 cues to the TO system will help define how STB hormone levels are mechanistically modulated.

683 In conclusion, our study elucidates STB nucleus subtypes in TOs, tracks their proportions across culture
684 conditions, and compares gene expression to STB *in vivo*. The fluctuating proportions of STB subtypes across

685 TO culture conditions imply that environmental cues can direct individual nuclei in the same cell into different
686 identities. These findings underscore the power of TOs as an experimental model for studying the STB.
687
688 **Methods:**
689 **Tissue Processing for SC and SN sequencing**
690 Placenta tissue was collected from patients undergoing scheduled C-sections at UNC Health consented under
691 IRB 21-2055. Patient information, sequencing data, and tissue samples from these experiments was later
692 transferred to Duke under the IRB Pro00113088. Immediately after placenta delivery a cotyledon from the
693 center of the placenta was dissected. Samples from both decidua and villous tissue were snap frozen in liquid
694 nitrogen for future processing within ten minutes of placenta delivery to minimize STB degradation. Additional
695 samples were fixed in 10% buffered formalin for subsequent tissue paraffin embedding and slicing. The
696 remaining villous/decidua tissue from the dissected cotyledon was then immediately processed into single cells,
697 as described below. A list of the tissues used in this study is available in **Supplementary Table 1**.
698 SC processing: The cotyledon (decidua + villous, chorion removed) was chopped into fine pieces (<1mm) with
699 a scalpel and washed with 1x PBS in cheese cloth until flow through was clear of blood. Tissue was placed into
700 Trypsin media (1X PBS without calcium or magnesium, 0.2% Trypsin (Thermo 15090046), 0.53M EDTA) and
701 incubated at 37°C for ten minutes in a shaking water bath. After incubation trypsin was inactivated with 100mLs
702 of Wash Media (DMEM F12 media + 20% FBS). Supernatant was passed through a sterile cheese cloth, spun
703 down, and resuspended to Resuspension Media (DMEM F12 media + 10% FBS). Remaining tissue was then
704 placed into 25mL collagenase buffer (1mg/mL collagenase V (Sigma C9263) in Wash Media) and shaken at
705 37°C for ten minutes. Supernatant was passed through cheese cloth, spun down, and resuspended in
706 Resuspension Media. Cell pellets from both digestion steps were combined and pelleted, resuspension media
707 removed, and resuspended in 10mLs RBC lysis buffer (Thermo 00-4333-57) and incubated at RT for 10min.
708 Cells were passed through a 100μm filter, spun down, and passed through a Milltenyi Debris Removal Solution
709 (130-109-398) gradient as per the manufacturer's instructions. The final pellet was then resuspended in 1X
710 PBS + 0.04% BSA (Sigma A1595).

711 SN processing: Single nuclei were isolated with the 10X Chromium Nuclear Isolation Kit (CG000505) as per
712 the User Guide with the following changes. 50mgs of frozen tissue was resuspended in lysis buffer on ice,
713 dounced to homogenize, and incubated for a total of only 7 minutes from the resuspension step to centrifugation.
714 In addition, while the initial centrifugation step in lysis buffer was performed at 500xg for 5 min to minimize time
715 spent in lysis buffer, subsequent wash spins were done at 500xg for 10min to minimize loss. The final pellet
716 was then resuspended in 1X PBS + 0.04% BSA (Sigma A1595) +10X Genomics supplied RNAse inhibitor.
717

718 **Organoid Culture**

719 STB^{in}, STB^{out}, and EVT^{enrich} TOs were derived, propagated, and differentiated as described previously (Yang
720 et al., 2022 and 2023). Briefly, STB^{in} TOs were derived and maintained by sequential digestion of term placental
721 chorionic villi with 0.2% trypsin-250 (Alfa Aesar, J63993), 0.02% EDTA (Sigma-Aldrich, E9884), and 1.0 mg/mL
722 collagenase V (STEMCELL Technologies, 100-0681), followed by further mechanical disruption by pipetting.
723 Pooled digests were washed with Advanced DMEM/F12 medium (Gibco 12634-010) and pelleted by
724 centrifugation, then resuspended in ice-cold Matrigel (Corning 356231). Matrigel "domes" (40 µl/well) were
725 plated into 24-well tissue culture plates (Corning 3526) and overlaid with 500 µL prewarmed term trophoblast
726 organoid medium (tTOM) (**Supplementary Table 3**). Cultures were maintained in 37°C humidified incubator
727 with 5% CO_2. Medium was renewed every 2-3 days. To generate STB^{out} TOs, mature STB^{in} TOs were released
728 from Matrigel domes with cell recovery solution (Corning, 354253) on ice for 30-60min, pelleted, washed one
729 time with cold basal media (Advanced DMEM/F12 + 1% P/S + 1% L-glutamine + 1% HEPES), and then
730 resuspended in pre-warmed tTOM supplemented with 5 µM Y-27632, and transferred into an ultra-low
731 attachment 24-well plate (Corning 3473) for suspension culture at 37℃ and 5% CO2 for 48 hours. To generate
732 EVT^{enrich} TOs, established STB^{in} TOs were passaged into new Matrigel "domes" as described above and
733 previously (Yang et al., 2022 eLife), and maintained in tTOM for ~ 5 days prior to switching to EVT differentiation
734 media 1 (EVT m1 recipe: **Supplementary Table 4**) for 9 days culture, then replaced with EVT m2 with the
735 same recipe as EVT m1, but lacking NRG1 for a further 3-4 days. A list of the TOs lines used in this study is
736 available in **Supplementary Table 1**.
737

738 **CRISPR/Cas9-mediated genes editing in TOs**

739 To generate *RYBP* and *AFF1* knock out TOs line, two sets of sgRNA pairs for each gene with the target sites
740 close to the 5 prime of genes ORF were selected from a pre-designed sgRNA database established by
741 Synthego (https://design.synthego.com/#/), then each sgRNA pair (dual-sgRNAs) were cloned into individual
742 cassettes on Lentiviral transfer plasmid with Cas9 ORF (Dual-gRNA lentivirus CRISPR vector). CRISPR
743 lentivirus was produced in 293T cells by the transient transfection of the combination of above genes specific
744 transfer plasmids, psPAX2 (packaging plasmids) and pMD2.G (envelop plasmids) at the ratio 2:1:1 following
745 the standard lentivirus packaging protocols described previously [1]. Using the prepared lentivirus, we transduced
746 the fully dissociated TO single-cell suspension overnight in an ultra-low attachment culture vessel. The cells
747 were then replated into fresh Matrigel domes for further culture and recovered forrecovery 2-4 days prior to
748 puromycin selection (2 μg/ml) for ~4 days. Single organoid unit picking and dissociation for clonal expansion
749 were performed after an additional two weeks of growth. Genomic DNA was purified from each individual single-
750 organoid clone for sequencing validation. High-fidelity PCR was conducted on the predicted target region of
751 the gRNAs using the primers listed in Supplemental Table 6. The purified PCR products were then subjected
752 to Sanger sequencing and analyzed by comparing them to sequences from scramble gRNA-mediated single-
753 organoid clones. Immunofluorescent staining was performed to further validate knockout single-organoid
754 clones. The sequences of the gRNAs used in this study can be found in Supplemental Table 5.

755

756 **Organoid Processing for SC and SN sequencing**

757 STB^{in} TOs were processed into both single cells and nuclei for SC/SN sequencing while STB^{out} and EVT^{enrich}
758 TOs were processed into single nuclei for SN sequencing via the following protocols.

759 <u>SC processing:</u> STB^{in} TOs were dissociated by scraping Matrigel domes into 1 mL of pre-warmed TrypLE
760 Express (Invitrogen, 12605036) and incubating at 37°C for 12 min, swirling the tube every 2-3 min. Dissociated
761 organoids were pelleted at 1250 rpm for 3 min and re-suspended in 200 μL DMEM containing 10% FBS.
762 Resuspended organoids were subjected to vigorous manual disruption using a single channel p200 pipette
763 (Ranin, 17008652) for 3 min followed by the addition of 800 μL of DMEM containing 10% FBS. The disrupted
764 suspension was then passed over a 40 μm filter cell strainer (Corning, 352098). Flow through was then

765 centrifuged at 1250 rpm for 5min and the pellet resuspended in 250 µL of 1x PBS for a final volume of ~300 µL
766 and cell counts of ~1 x 10^6 cells/mL.
767 SN processing: TOs from each condition (STB^{in}, STB^{out}, EVT^{enrich}) were harvested by scraping with a wide bore
768 pipette, centrifuged to pellet (600xg for 6min), resuspended in 100uls TrypLE (Thermo Fisher, 12605010), and
769 incubated at 37ºC for 10min. After incubation each sample was pipetted 100x with a P200 pipette to dissociate
770 cells and placed on ice. Single nuclei were then isolated with the 10x Chromium Nuclear Isolation Kit
771 (CG000505) as per the User Guide with the following changes. 500uls of Lysis buffer was added to the
772 TO/TrypLE solution and transferred to a 2mL Kimble Dounce (Millipore Sigma, D8938) on ice, dounced 10x,
773 and subsequently incubated on ice for a total of 10 minutes. Remaining steps were performed as suggested,
774 except for final wash step spins were performed at 500xg for 10min to minimize nuclei loss. The final pellet was
775 then resuspended in 10mLs of 1X PBS + 0.04% BSA (Sigma A1595) +10X Genomiocs supplied RNAse
776 inhibitor, nuclei counted, and 10,000 nuclei run in each well of a chromium controller.
777
778 **10X Genomics library generation, sequencing, and data analysis**
779 SC suspensions were stained with Trypan Blue and counted to obtain live/dead cell ratios while SN were
780 stained with Ethidium Homodimer-1 (Thermo E1169) and counted with a hemocytometer on a fluorescent
781 microscope. 10,000 SC/SN of each sample type were loaded into individual chip wells and run on a 10x
782 chromium controller with the Chromium Single Cell 3' Reagent Reagent Kit v3.1 (Dual Index) following the
783 manufacturers protocol. Tissue libraries were then sequenced on an Illumina NovaSeq S2 at a targeted
784 sequencing depth of 100,000 reads/cell or nucleus while organoid libraries were sequenced on an Illumna
785 NovaSeq S4 at a targeted sequencing depth of 74,000 reads/cell or nucleus. Cell Ranger was then used to
786 align reads to the human genome (GRCh38) and create a counts matrix.
787 SC and SN Data Analysis: Post-processing, quality control, and read alignment to the hg38 human reference
788 genome were performed using 10x CellRanger package (v6.1.2, 10x Genomics). Gene expression matrices
789 generated by the 10x CellRanger aggregate option were analyzed using Seurat (version 4.0) in R [2-5]. For SC,
790 cells with at least 200 and no more than 10,000 unique expressed genes were included in downstream analysis,
791 and cells with more than 25% mitochondrial reads were excluded from analysis. For SN, nuclei with at least

792 800 and no more than 10,000 unique features and less than 60,000 counts were included in downstream
793 analysis, and nuclei with more than 7.5% mitochondrial reads and 3% ribosomal reads were excluded from
794 analysis. To eliminate batch effects, datasets from unique donors were normalized using the *sctransform*
795 function (version 2) and integrated using the *FindIntegrationAnchors()* in Seurat (version 4.0) in R [5]. Variables
796 regressed included nFeatures, nCounts, percent mitochondria and ribosomes, and X- and Y-linked genes to
797 avoid sex-associated differences. Dimensional reduction was performed using the *RunPCA()* function to obtain
798 the first 40 principal components, which was determined using *ElbowPlots()* across the first 50 dimensions. To
799 identify clusters, Louvain clustering (Seurat *FindClusters()* function) was performed, and optimal resolution was
800 determined using the *clustree()* function [6] on a range of resolutions between 0.2-1.0, with 0.6 selected for TOs
801 and 0.3 selected for tissue. To identify clusters enriched in combined files of TOs and tissue, dataset integration
802 was performed using Harmony and Louvain clustering (Seurat) performed at a 0.3 resolution, as optimized
803 using *clustree()* [6]. Differential expression analysis between clusters was performed using the Wilcoxon rank
804 sum test (Seurat) using *FindAllMarkers()*, with genes with a $\log_2$ fold change threshold set to 0.25 and FDR-
805 adjusted p-value < 0.05 considered significant. Pseudobulk differential expression analysis was performed
806 using DESeq2 (Love et al,). GO term enrichment was performed with clusterProfiler using *compareCluster.*
807 <u>Pseudotime:</u> The *slingshot* package (version 2.6.0) in R was used to determine differentiation trajectories from
808 clusters identified in Seurat with unbiased starting and ending roots [7]. The raw counts and above-generated
809 slingshot object were used to run *evaluateK()* with the total number of knots ranging from 3 to 9. The optimal
810 number of knots was determined to be 5. The *fitGAM()* function using *tradeSeq* (1.5.10) was run with this
811 resulting value and gene expression along lineages identified using the *associationTest()* function [8]. Heatmaps
812 of expression changes across lineages were generated using *ComplexHeatmap()* on log transformed counts
813 and rasterized using the *ImageMagick* "Bessel" filter [9]. The *plotGenePseudotime()* function was used to
814 visualize raw count gene expression in individual cells across lineages from the *slingshot* object.
815 <u>RNA Velocity and Velorama:</u> RNA velocity was performed via the python based program scVelo on snRNAseq
816 data from both placenta tissues of three patients and organoids from three patient-derived TO cell lines (Bergen
817 et al., 2020). The organoids were further divided into STB^{in} and STB^{out} subcategories, resulting in nine total
818 datasets in our analysis. First, we generated UMAPs for each data source (full-term tissue, STB^{in}, and STB^{out})

819 with corresponding trajectory vectors. For the TOs we included only the CTB, CTB-pf, and STB nucleus types
820 in the analysis. For each data source, the sample datasets were integrated with Scanorama to eliminate
821 dataset-specific batch effects for transcript counts as well as spliced and unspliced transcripts (Hie et al., 2018).
822 The samples were then merged and UMAPs with trajectory vectors were created using the scVelo library. Then,
823 we employed Geosketch to downsample the cell population represented in the UMAP while preserving
824 transcriptomic heterogeneity (Hie et al., 2019). This was done to enhance the clarity and distinction of cells on
825 the UMAP. Second, we inferred gene regulatory networks with Velorama (Singh et al., 2024). We compiled
826 lists of human transcription factors (TFs) and genes coding for chromatin remodelers (CRs) from sources like
827 https://www.factorbook.org/tf/human to use as regulatory genes, along with a selection of highly variable genes
828 and genes of interest from the tissue and organoid datasets to use as our target genes. Velorama was then
829 used to infer the gene regulatory networks under default settings and produced a total of nine regulatory-target
830 gene interaction matrices for tissues and organoids raw data sets. Each interaction matrix provides scores that
831 highlight the strength of the relationship between specific regulatory-target gene pairs. We then ranked the
832 regulatory-target gene pairs by their interaction strength and identified top TFs in each sample, after filtering
833 TFs by number of target genes among the top 500 pairs. Heatmaps were then created based on the overlap
834 of target genes with a score of 1 representing total overlap and a score of 0 indicating no overlap. Finally, top
835 target genes in each cluster were found via sorting by interaction score and plotted as a network analysis with
836 the R package igraph, with the width of the arrow representing the Velorama interaction strength score.
837

838 **RNA extraction and bulk RNA-seq analysis**

839 Total RNA from TOs was purified with the Sigma GenElute Universal total RNA purification kit (Sigma-Aldrich,
840 RNB100) following manufacturer's instruction. Purified Total RNA concentration and quality was determined
841 by Thermo scientific Nanodrop one. All RNA samples submitted for bulk RNA-seq were further run for QC
842 evaluation for their RQN (RNA quality number, 10 for all samples) prior to library preparation by the Duke
843 Sequencing and Genomic Technologies (SGT) using KAPA HyperPrep kit (Roche). Sequencing was performed
844 on the NextSeq 1000 XLEAP using P2 flow cell. The reads were aligned to the human reference genome
845 (GRCh38) using QIAGEN CLC Genomics (v20). Differential expression analysis was performed using the

846 DESeq2 package in R with significance cutoff as 0.05 and fold change cutoff at $\log_2 \pm 2$ [10]., Files associated
847 with bulk RNA-seq studies have been deposited into Sequence Read Archive (GSE288650). Volcano plots
848 were generated using the EnhancedVolcano package in R [11] or in Graphpad Prism version 9.

849 **Immunofluorescence in placenta tissue**

850 FFPE tissue sections derived from the same patients sequenced in Figure 1 were removed from paraffin and
851 rehydrated via an iteration through the following 3min wash steps (Xylene, Xylene, 1:1 Xylene:100% EtOH,
852 100% EtOH, 100% EtOH, 95% EtOH, 70% EtOH, 50% EtOH). Slides were then placed under running tap water
853 for 5 minutes to re-hydrate then transferred to sodium citrate buffer (10mM sodium citrate, 0.05% Tween 20,
854 pH6) and placed into boiling water for 20min for antigen revival. Slides were then placed under running tap
855 water for 10minutes then transferred into PBS. To perform IF, tissue was permeabilized with 0.5% Triton X-
856 100 in 1X PBS for 20min at RT then washed 2x in 1X PBS. Reb blood cell autofluorescence was quenched
857 with TrueBlack Lipofuscin Autofluorescence Quencher (Biotium #2300) as per the manufacturer's instructions
858 then washed 2x in 1X PBS. Tissue slides were then blocked in blocking buffer (1% BSA in 1X PBS) for 1 hour
859 at RT. Primary antibodies were then incubated overnight at 4℃ in 0.1% BSA in 1x PBS in the following dilutions:
860 1:1000 RYBP (Millipore Sigma HPA053357), 1:500 Cytokeratin-7 (Millipore Sigma MABT1490), and 1:200 E-
861 cadherin (BD Biosciences 610181). Slides were rinsed 2x in 1X PBS, and incubated in secondary antibodies
862 for 1 hour at 37℃ (Invitrogen A-21247, A-11011, A-11001). Slides were rinsed 2x in 1X PBS, incubated in 1
863 µg/ml Hoechst in 1X PBS for ten minutes at RT, and finally washed 1x in 1X PBS. PBS was then removed and
864 slides mounted with ProLong Diamond Antifade (Thermo P36965) and dried overnight prior to imaging. Slides
865 were imaged on a Nikon Ti-E stand equipped with a Yokogawa CSU-W1 spinning disk confocal unit with a 40x
866 Nikon Silicone objective and illuminated with 405/488/565/646 laser sources.

867

868 **Cryosectioning and immunofluorescence staining of TOs**

869 TOs were collected in microcentrifuges tubes pre-coated with regular FBS, then rinsed once with 1X PBS prior
870 to fixing in 4% PFA at RT for 2 h. Pelleted TOs were washed twice with 1X PBS and resuspended in 1X PBS
871 with 0.5 mL 20% (wt/vol) sucrose solution per sample, then transferred to 4℃ overnight to allow all the organoid
872 units to pellet into the bottom of sucrose solution. On the following day, 7.5% gelatin (wt/vol)/10% (wt/vol)

873 sucrose embedding solution was pre-warmed at 37℃ for 30 min, then organoid units were isolated from sucrose
874 solution into small size molds (7×7×5 mm) and polymerize with embedding solution at 4 ℃ for 20 min before
875 transferring into -80 ℃ for at least 3 hrs prior to cryosectioning.
876 To section above prepared organoid frozen blocks, the blocks were transferred from -80℃ into the cryosection
877 machine (Leica CM1950 Cryostat) at -20℃ to equilibrate for 15 min, then 10 μm thickness sections cut. The
878 cryosections were incubated at RT for 15 min before incubation in permeabilization buffer (0.5% <vol/vol>
879 Trition X-100 in 1X PBS with or without 5% <wt/vol> goat serum) for 45 min at RT. Cryosections were washed
880 and blocked in 5%(v/v) goat serum or BSA/0.1%(v/v) Tween-20 in 1X PBS for 15 min at RT and then incubated
881 with rabbit anti-human RYBP polyclonal antibody (Sigma, HPA053357), mouse anti-human hCG-β antibody
882 (abcam, ab9582), rat anti-human E-cadherincadherin (Thermo Fisher 14-3249-82) diluted in above-described
883 blocking solution at 4℃ overnight. The following day cryosections were washed with 1X PBS and then
884 incubated for 1 h at RT with Multi-rAb CoraLite Plus 488 Goat anti-mouse (Proteintech, RGAM002), Multi-rAb
885 CoraLite Plus 594 Goat anti-rabbit (Proteintech, RGAR004), and either Donkey Anti-Rat IgG H&L (Alexa Fluor®
886 647) preadsorbed (Abcam ab150155) recombinant secondary antibodies or Alexa Fluor 647–conjugated
887 phalloidin (Invitrogen, A22287). Cryosections were washed again with 1X PBS and mounted in Vectashield
888 (Vector Laboratories, H-1200) containing 4′,6-diamidino- 2-phenylindole (DAPI). Images were captured using
889 a Olympus Fluoview FV3000 inverted confocal microscope or a Nikon-Yokogawa CSU-W1 spinning disk
890 confocal and contrast-adjusted in Photoshop or Fiji.
891
892 **Cryosectioning and RNA fluorescence in situ hybridization (FISH) of TOs**
893 TOs were collected in microcentrifuge tubes pre-coated with 1 mg/mL BSA, rinsed once with 1X PBS, and
894 fixed in 4% PFA at RT for 30 minutes. After fixation, TOs were pelleted, washed twice with 1X PBS, and
895 embedded in OCT within a cryomold. The embedded samples were then flash-frozen in 2-methylbutane and
896 stored at -80℃. Cryosections (10 μm thick) were cut using a cryostat and transferred onto microscope slides
897 (Thermo Fisher 12-550-15). To remove OCT, sections were washed three times with 1X PBS, followed by
898 permeabilization in 0.5% Triton X-100 in 1X PBS for 45 minutes at RT. After two additional PBS washes,
899 sections were incubated for 30 minutes in 30% formamide wash buffer (30% vol/vol formamide in 2X saline-

900 sodium citrate (SCC) buffer). For primary probe hybridization, TO sections were incubated overnight at 37℃
901 in 30% hybridization buffer (30% (vol/vol) formamide, 1 mg/mL yeast tRNA, and 10% (wt/vol) dextran sulfate
902 in 2X SCC buffer) with 1μM primary FISH probes targeting either PAPPA2 or ADAMTS6 (**Supplemental**
903 **Table 7**). The next day, sections were washed twice with 30% formamide wash buffer at 47℃ for 30 minutes,
904 followed by a 5-minute incubation in 10% formamide wash buffer (10% vol/vol formamide in 2X SCC buffer).
905 Next, TO sections were incubated for 1 hour at 37℃ with 5 nM of each secondary probe (bit1_5pCy5,
906 bit11_5pCy5, bit12_5pCy5) in 10% hybridization buffer (**Supplemental Table 7**). Following secondary probe
907 hybridization, sections were washed three times in 10% formamide wash buffer for 5 minutes each at room
908 temperature. During the second wash, nuclei were counterstained with 1 μg/mL DAPI or Hoechst diluted in
909 10% hybridization buffer. Finally, TO sections were mounted in Prolong Diamond Antifade (Thermo Fisher
910 P36970) and imaged using a Nikon Ti-E stand equipped with a Yokogawa CSU-W1 spinning disk confocal
911 unit. Imaging was performed with a 100× Nikon silicone objective under 405/646 laser illumination.

912 **Data Availability:** The datasets analyzed in this paper can be accessed on GEO with the accession number
913 GSE288650. In addition, the processed datasets can be interactively visualized online at
914 https://gladfelterlab.shinyapps.io/PlacentaRNAsequencing/.

915 **Acknowledgements**

916 We thank Jennifer Gilner, Jillian Hurst, and the Project Hope1000 (Duke University) for providing placental
917 tissue used to derive organoids in this work. We thank Karen Dorman, Neeta Vora, Charles Perou, and
918 Michelle Hayward at UNC Chapel Hill for their assistance in obtaining IRB approval and placenta tissues at
919 UNC CH. This project was supported by NIH AI145828 (CBC), an HHMI Faculty Scholar award (ASG), NSF
920 743900 (ASG). The organoid work performed by MMK was supported by NIH K00CA245719. We thank the
921 Duke University School of Medicine for the use of the Sequencing and Genomic Technologies Shared
922 Resource and the Translational Genomics Lab at UNC Chapel Hill Lineberger Comprhensive Cancer Center,
923 both of which provided RNA-seq services.

924

925 **Bibliography**

926 Aghababaei, M., Hogg, K., Perdu, S., Robinson, W.P., Beristain, A.G., 2015. ADAM12-directed ectodomain
927 shedding of E-cadherin potentiates trophoblast fusion. Cell Death Differ. 22, 1970–1984.
928 https://doi.org/10.1038/cdd.2015.44

929 Arutyunyan, A., Roberts, K., Troulé, K., Wong, F.C.K., Sheridan, M.A., Kats, I., Garcia-Alonso, L., Velten, B.,
930 Hoo, R., Ruiz-Morales, E.R., Sancho-Serra, C., Shilts, J., Handfield, L.-F., Marconato, L., Tuck, E.,
931 Gardner, L., Mazzeo, C.I., Li, Q., Kelava, I., Wright, G.J., Prigmore, E., Teichmann, S.A., Bayraktar, O.A.,
932 Moffett, A., Stegle, O., Turco, M.Y., Vento-Tormo, R., 2023. Spatial multiomics map of trophoblast
933 development in early pregnancy. Nature 616, 143–151. https://doi.org/10.1038/s41586-023-05869-0

934 Aye, I.L.M.H., Aiken, C.E., Charnock-Jones, D.S., Smith, G.C.S., 2022. Placental energy metabolism in
935 health and disease—significance of development and implications for preeclampsia. Am. J. Obstet.
936 Gynecol. 226, S928–S944. https://doi.org/10.1016/j.ajog.2020.11.005

937 Baczyk, D., Satkunaratnam, A., Nait-Oumesmar, B., Huppertz, B., Cross, J.C., Kingdom, J.C.P., 2004.
938 Complex Patterns of GCM1 mRNA and Protein in Villous and Extravillous Trophoblast Cells of the Human
939 Placenta. Placenta 25, 553–559. https://doi.org/10.1016/j.placenta.2003.12.004

940 Bai, X., Lenhart, K.C., Bird, K.E., Suen, A.A., Rojas, M., Kakoki, M., Li, F., Smithies, O., Mack, C.P., Taylor,
941 J.M., 2013. The smooth muscle-selective RhoGAP GRAF3 is a critical regulator of vascular tone and
942 hypertension. Nat. Commun. 4, 2910–2910. https://doi.org/10.1038/ncomms3910

943 Barker, S.B., Cumming, G., Horsfield, K., 1973. Quantitative morphometry of the branching structure of trees.
944 J. Theor. Biol. 40, 33–43. https://doi.org/10.1016/0022-5193(73)90163-x

945 Barrios, V., Chowen, J.A., Martín-Rivada, Á., Guerra-Cantera, S., Pozo, J., Yakar, S., Rosenfeld, R.G.,
946 Pérez-Jurado, L.A., Suárez, J., Argente, J., 2021. Pregnancy-Associated Plasma Protein (PAPP)-A2 in
947 Physiology and Disease. Cells 10, 3576. https://doi.org/10.3390/cells10123576

948 Beck, T., Schweikhart, G., Stolz, E., 1986. Immunohistochemical location of HPL, SP1 and β-HCG in normal
949 placentas of varying gestational age. Arch Gynecol 239, 63–74. https://doi.org/10.1007/bf02133965

950 Bégay, V., Smink, J., Leutz, A., 2004. Essential Requirement of CCAAT/Enhancer Binding Proteins in
951 Embryogenesis. Mol. Cell. Biol. 24, 9744–9751. https://doi.org/10.1128/mcb.24.22.9744-9751.2004

952 Benirschke, K., Burton, G.J., Baergen, R.N., 2012. Pathology of the Human Placenta 761–880.
953 https://doi.org/10.1007/978-3-642-23941-0_25

954 Bergen, V., Lange, M., Peidli, S., Wolf, F.A., Theis, F.J., 2020. Generalizing RNA velocity to transient cell
955 states through dynamical modeling. Nat. Biotechnol. 38, 1408–1414. https://doi.org/10.1038/s41587-020-
956 0591-3

957 Boyd, J.D., Hamilton, W.J., 1970. The Human Placenta. https://doi.org/10.1007/978-1-349-02807-8

958 Burgos, M.H., Rodríguez, E.M., 1966. Specialized zones in the trophoblast of the human term placenta. Am J
959 Obstet Gynecol 96, 342–356. https://doi.org/10.1016/0002-9378(66)90237-7

960 Burton, G.J., 1990. On the varied appearances of the human placental villous surface visualised by scanning
961 electron microscopy. Scanning Microscopy 4, 501–7.

962 Burton, G.J., Jauniaux, E., 1995. Sonographic, stereological and Doppler flow velocimetric assessments of
963 placental maturity. Bjog Int J Obstetrics Gynaecol 102, 818–825. https://doi.org/10.1111/j.1471-
964 0528.1995.tb10849.x

965 Butler, A., Hoffman, P., Smibert, P., Papalexi, E., Satija, R., 2018. Integrating single-cell transcriptomic data
966 across different conditions, technologies, and species. Nat. Biotechnol. 36, 411–420.
967 https://doi.org/10.1038/nbt.4096

968 Cain, S.A., Mularczyk, E.J., Singh, M., Massam-Wu, T., Kielty, C.M., 2016. ADAMTS-10 and -6 differentially
969 regulate cell-cell junctions and focal adhesions. Sci. Rep. 6, 35956. https://doi.org/10.1038/srep35956

970 Cain, S.A., Woods, S., Singh, M., Kimber, S.J., Baldock, C., 2022. ADAMTS6 cleaves the large latent TGFβ
971 complex and increases the mechanotension of cells to activate TGFβ. Matrix Biol. 114, 18–34.
972 https://doi.org/10.1016/j.matbio.2022.11.001

973 Chen, Y., Siriwardena, D., Penfold, C., Pavlinek, A., Boroviak, T.E., 2022. An integrated atlas of human
974 placental development delineates essential regulators of trophoblast stem cells. Dev. (Camb., Engl.) 149,
975 dev200171. https://doi.org/10.1242/dev.200171

976 Ching, Y.-P., Wong, C.-M., Chan, S.-F., Leung, T.H.-Y., Ng, D.C.-H., Jin, D.-Y., Ng, I.O., 2003. Deleted in
977 Liver Cancer (DLC) 2 Encodes a RhoGAP Protein with Growth Suppressor Function and Is
978 Underexpressed in Hepatocellular Carcinoma*. J. Biol. Chem. 278, 10824–10830.
979 https://doi.org/10.1074/jbc.m208310200

980 Clark, D., Smith, S., Licence, D., Evans, A., Charnock-Jones, D., 1998. Comparison of expression patterns
981 for placenta growth factor, vascular endothelial growth factor (VEGF), VEGF-B and VEGF-C in the human
982 placenta throughout gestation. J Endocrinol 159, 459–467. https://doi.org/10.1677/joe.0.1590459

983 Costa, M.A., 2016. The endocrine function of human placenta: an overview. Reprod Biomed Online 32, 14–
984 43. https://doi.org/10.1016/j.rbmo.2015.10.005

985 Derisoud, E., Jiang, H., Zhao, A., Chavatte-Palmer, P., Deng, Q., 2024. Revealing the molecular landscape
986 of human placenta: a systematic review and meta-analysis of single-cell RNA sequencing studies. Hum.
987 Reprod. Updat. dmae006. https://doi.org/10.1093/humupd/dmae006

988 Foxler, D.E., Bridge, K.S., Foster, J.G., Grevitt, P., Curry, S., Shah, K.M., Davidson, K.M., Nagano, A.,
989 Gadaleta, E., Rhys, H.I., Kennedy, P.T., Hermida, M.A., Chang, T., Shaw, P.E., Reynolds, L.E., McKay,
990 T.R., Wang, H., Ribeiro, P.S., Plevin, M.J., Lagos, D., Lemoine, N.R., Rajan, P., Graham, T.A., Chelala,
991 C., Hodivala-Dilke, K.M., Spendlove, I., Sharp, T.V., 2018. A HIF–LIMD1 negative feedback mechanism
992 mitigates the pro-tumorigenic effects of hypoxia. EMBO Mol. Med. 10, e8304.
993 https://doi.org/10.15252/emmm.201708304

994 Haeussner, E., Buehlmeyer, A., Schmitz, C., Koch, F.E. von, Frank, H.-G., 2014. Novel 3D Microscopic
995 Analysis of Human Placental Villous Trees Reveals Unexpected Significance of Branching Angles. Sci.
996 Rep. 4, 6192. https://doi.org/10.1038/srep06192

997 Haider, S., Meinhardt, G., Saleh, L., Kunihs, V., Gamperl, M., Kaindl, U., Ellinger, A., Burkard, T.R., Fiala, C.,
998 Pollheimer, J., Mendjan, S., Latos, P.A., Knöfler, M., 2018. Self-Renewing Trophoblast Organoids
999 Recapitulate the Developmental Program of the Early Human Placenta. Stem Cell Rep 11, 537–551.
000 https://doi.org/10.1016/j.stemcr.2018.07.004

001 Hao, Y., Hao, S., Andersen-Nissen, E., Mauck, W.M., Zheng, S., Butler, A., Lee, M.J., Wilk, A.J., Darby, C.,
002 Zager, M., Hoffman, P., Stoeckius, M., Papalexi, E., Mimitou, E.P., Jain, J., Srivastava, A., Stuart, T.,
003 Fleming, L.M., Yeung, B., Rogers, A.J., McElrath, J.M., Blish, C.A., Gottardo, R., Smibert, P., Satija, R.,
004 2021. Integrated analysis of multimodal single-cell data. Cell 184, 3573-3587.e29.
005 https://doi.org/10.1016/j.cell.2021.04.048

006 Hatterschide, J., Natale, C.A., Ridky, T.W., and White, E.A. (2023). Monitoring cell fate in 3D organotypic
007 human squamous epithelial cultures. STAR Protoc 4, 102101. http:// doi: 10.1016/j.xpro.2023.102101.

008 Hemberger, M., Hanna, C.W., Dean, W., 2020. Mechanisms of early placental development in mouse and
009 humans. Nat. Rev. Genet. 21, 27–43. https://doi.org/10.1038/s41576-019-0169-4

010 Hempstock, J., Bao, Y.-P., Bar-Issac, M., Segaren, N., Watson, A.L., Charnock-Jones, D.S., Jauniaux, E.,
011 Burton, G.J., 2003. Intralobular Differences in Antioxidant Enzyme Expression and Activity Reflect the
012 Pattern of Maternal Arterial Bloodflow Within the Human Placenta. Placenta 24, 517–523.
013 https://doi.org/10.1053/plac.2002.0955

014 Hie, B., Bryson, B., Berger, B., 2018. Efficient integration of heterogeneous single-cell transcriptomes using
015 Scanorama. Nat. Biotechnol. 37, 685–691. https://doi.org/10.1038/s41587-019-0113-3

016 Hie, B., Cho, H., DeMeo, B., Bryson, B., Berger, B., 2019. Geometric Sketching Compactly Summarizes the
017 Single-Cell Transcriptomic Landscape. Cell Syst. 8, 483-493.e7. https://doi.org/10.1016/j.cels.2019.05.003

018 ImageMagick. ImageMagick Studio LLC. 2023. Available from: https://imagemagick.org.

019 Jauniaux, E., Hempstock, J., Greenwold, N., Burton, G.J., 2003. Trophoblastic Oxidative Stress in Relation to
020 Temporal and Regional Differences in Maternal Placental Blood Flow in Normal and Abnormal Early
021 Pregnancies. Am J Pathology 162, 115–125. https://doi.org/10.1016/s0002-9440(10)63803-5

022 Khaliq, A., Li, X.F., Shams, M., Sisi, P., Acevedo, C.A., Whittle, M.J., Weigh, H., Ahmed, A., 2009.
023 Localisation of Placenta Growth Factor (PlGF) in Human Term Placenta. Growth Factors 13, 243–250.
024 https://doi.org/10.3109/08977199609003225

025 Kim, M., Franke, V., Brandt, B., Lowenstein, E.D., Schöwel, V., Spuler, S., Akalin, A., Birchmeier, C., 2020.
026 Single-nucleus transcriptomics reveals functional compartmentalization in syncytial skeletal muscle cells.
027 Nat Commun 11, 6375. https://doi.org/10.1038/s41467-020-20064-9

028 Kumar, P., Magon, N., 2012. Hormones in pregnancy. Niger. Méd. J. : J. Niger. Méd. Assoc. 53, 179–183.
029 https://doi.org/10.4103/0300-1652.107549

030 Li, F., Long, Y., Yu, X., Tong, Y., Gong, L., 2022. Different Immunoregulation Roles of Activin A Compared
031 With TGF-β. Front. Immunol. 13, 921366. https://doi.org/10.3389/fimmu.2022.921366

032 Li, Q., Sharkey, A., Sheridan, M., Magistrati, E., Arutyunyan, A., Huhn, O., Sancho-Serra, C., Anderson, H.,
033 McGovern, N., Esposito, L., Fernando, R., Gardner, L., Vento-Tormo, R., Turco, M.Y., Moffett, A., 2024.
034 Human uterine natural killer cells regulate differentiation of extravillous trophoblast early in pregnancy. Cell
035 Stem Cell 31, 181-195.e9. https://doi.org/10.1016/j.stem.2023.12.013

036 Li, X., Li, Z.-H., Wang, Y.-X., Liu, T.-H., 2023. A comprehensive review of human trophoblast fusion models:
037 recent developments and challenges. Cell Death Discov. 9, 372. https://doi.org/10.1038/s41420-023-
038 01670-0

039 Li, Y., Moretto-Zita, M., Leon-Garcia, S., Parast, M.M., 2014. p63 Inhibits Extravillous Trophoblast Migration
040 and Maintains Cells in a Cytotrophoblast Stem Cell-Like State. Am. J. Pathol. 184, 3332–3343.
041 https://doi.org/10.1016/j.ajpath.2014.08.006

042 Liu, Y., Fan, X., Wang, R., Lu, X., Dang, Y.-L., Wang, Huiying, Lin, H.-Y., Zhu, C., Ge, H., Cross, J.C., Wang,
043 Hongmei, 2018. Single-cell RNA-seq reveals the diversity of trophoblast subtypes and patterns of
044 differentiation in the human placenta. Cell Res 28, 819–832. https://doi.org/10.1038/s41422-018-0066-y

045 Love, M.I., Huber, W., Anders, S., 2014. Moderated estimation of fold change and dispersion for RNA-seq
046 data with DESeq2. Genome Biol. 15, 550. https://doi.org/10.1186/s13059-014-0550-8

047 Manno, G.L., Soldatov, R., Zeisel, A., Braun, E., Hochgerner, H., Petukhov, V., Lidschreiber, K., Kastriti,
048 M.E., Lönnerberg, P., Furlan, A., Fan, J., Borm, L.E., Liu, Z., Bruggen, D. van, Guo, J., He, X., Barker, R.,
049 Sundström, E., Castelo-Branco, G., Cramer, P., Adameyko, I., Linnarsson, S., Kharchenko, P.V., 2018.
050 RNA velocity of single cells. Nature 560, 494–498. https://doi.org/10.1038/s41586-018-0414-6

051 Marsh, B., Zhou, Y., Kapidzic, M., Fisher, S., Blelloch, R., 2022. Regionally distinct trophoblast regulate
052 barrier function and invasion in the human placenta. eLife 11, e78829. https://doi.org/10.7554/elife.78829

053 Mayhew, T.M., 2014. Turnover of human villous trophoblast in normal pregnancy: What do we know and
054 what do we need to know? Placenta 35, 229–240. https://doi.org/10.1016/j.placenta.2014.01.011

055 Mayhew, T.M., Simpson, R.A., 1994. Quantitative evidence for the spatial dispersal of trophoblast nuclei in
056 human placental villi during gestation. Placenta 15, 837–44. https://doi.org/10.1016/s0143-
057 4004(05)80185-7

058 Megli, C.J., Coyne, C.B., 2021. Infections at the maternal–fetal interface: an overview of pathogenesis and
059 defence. Nat Rev Microbiol 1–16. https://doi.org/10.1038/s41579-021-00610-y

060 Mizutani, T., Orisaka, M., Miyazaki, Y., Morichika, R., Uesaka, M., Miyamoto, K., Yoshida, Y., 2022. Inhibition
061 of YAP/TAZ-TEAD activity induces cytotrophoblast differentiation into syncytiotrophoblast in human
062 trophoblast. Mol. Hum. Reprod. 28, gaac032. https://doi.org/10.1093/molehr/gaac032

063 Moore, T., Williams, J.M., Becerra-Rodriguez, M.A., Dunne, M., Kammerer, R., Dveksler, G., 2021.
064 Pregnancy-specific glycoproteins: evolution, expression, functions and disease associations. Reprod.
065 (Camb., Engl.) 163, R11–R23. https://doi.org/10.1530/rep-21-0390

066 Morrish, D.W., Marusyk, H., 1997. Localization of human chorionic gonadotropin and placental lactogen by
067 immunogold labeling for electron microscopy: Technique and limitations. Microsc Res Techniq 38, 176–
068 187. https://doi.org/10.1002/(sici)1097-0029(19970701/15)38:1/2<176::aid-jemt18>3.0.co;2-m

069 Mouzon, S.H., 1997. The GLUT3 Glucose Transporter Isoform Is Differentially Expressed within Human
070 Placental Cell Types. J Clin Endocr Metab 82, 2689–2694. https://doi.org/10.1210/jc.82.8.2689

071 Okae, H., Toh, H., Sato, T., Hiura, H., Takahashi, S., Shirane, K., Kabayama, Y., Suyama, M., Sasaki, H.,
072 Arima, T., 2018. Derivation of Human Trophoblast Stem Cells. Cell Stem Cell 22, 50-63.e6.
073 https://doi.org/10.1016/j.stem.2017.11.004

074 Pique-Regi, R., Romero, R., Tarca, A.L., Sendler, E.D., Xu, Y., Garcia-Flores, V., Leng, Y., Luca, F., Hassan,
075 S.S., Gomez-Lopez, N., 2019. Single cell transcriptional signatures of the human placenta in term and
076 preterm parturition. Elife 8, e52004. https://doi.org/10.7554/elife.52004

077 Pirity, M.K., Locker, J., Schreiber-Agus, N., 2005. Rybp/DEDAF Is Required for Early Postimplantation and
078 for Central Nervous System Development. Mol. Cell. Biol. 25, 7193–7202.
079 https://doi.org/10.1128/mcb.25.16.7193-7202.2005

080 Qu, H., Khalil, R.A., 2022. Role of ADAM and ADAMTS disintegrin and metalloproteinases in normal
081 pregnancy and preeclampsia. Biochem. Pharmacol. 206, 115266.
082 https://doi.org/10.1016/j.bcp.2022.115266

083 Rodriguez, M.A. de la R., Kersten, S., 2020. Regulation of lipid droplet homeostasis by hypoxia inducible lipid
084 droplet associated HILPDA. Biochim. Biophys. Acta (BBA) - Mol. Cell Biol. Lipids 1865, 158738.
085 https://doi.org/10.1016/j.bbalip.2020.158738

086 Rose, N.R., King, H.W., Blackledge, N.P., Fursova, N.A., Ember, K.J., Fischer, R., Kessler, B.M., Klose, R.J.,
087 2016. RYBP stimulates PRC1 to shape chromatin-based communication between Polycomb repressive
088 complexes. eLife 5, e18591. https://doi.org/10.7554/elife.18591

089 Rull, K., Laan, M., 2005. Expression of β-subunit of HCG genes during normal and failed pregnancy. Hum.
090 Reprod. 20, 3360–3368. https://doi.org/10.1093/humrep/dei261

091 SAMAAN, N., YEN, S.C.C., FRIESEN, H., PEARSON, O.H., 1966. Serum Placental Lactogen Levels During
092 Pregnancy and in Trophoblastic Disease. J. Clin. Endocrinol. Metab. 26, 1303–1308.
093 https://doi.org/10.1210/jcem-26-12-1303

094 Sasagawa, T., Nagamatsu, T., Morita, K., Mimura, N., Iriyama, T., Fujii, T., Shibuya, M., 2018. HIF-2α, but
095 not HIF-1α, mediates hypoxia-induced up-regulation of Flt-1 gene expression in placental trophoblasts.
096 Sci. Rep. 8, 17375. https://doi.org/10.1038/s41598-018-35745-1

097 Sasagawa, T., Nagamatsu, T., Yanagisawa, M., Fujii, T., Shibuya, M., 2021. Hypoxia-inducible factor-1β is
098 essential for upregulation of the hypoxia-induced FLT1 gene in placental trophoblasts. Mol. Hum. Reprod.
099 27, gaab065. https://doi.org/10.1093/molehr/gaab065

100 Satija, R., Farrell, J.A., Gennert, D., Schier, A.F., Regev, A., 2015. Spatial reconstruction of single-cell gene
101 expression data. Nat. Biotechnol. 33, 495–502. https://doi.org/10.1038/nbt.3192

102 Shannon, M.J., McNeill, G.L., Koksal, B., Baltayeva, J., Wächter, J., Castellana, B., Peñaherrera, M.S.,
103 Robinson, W.P., Leung, P.C.K., Beristain, A.G., 2024. Single-cell assessment of primary and stem cell-
104 derived human trophoblast organoids as placenta-modeling platforms. Dev. Cell 59, 776-792.e11.
105 https://doi.org/10.1016/j.devcel.2024.01.023

106 Sharkey, A.M., Charnock-Jones, D.S., Boocock, C.A., Brown, K.D., Smith, S.K., 1993. Expression of mRNA
107 for vascular endothelial growth factor in human placenta. Reproduction 99, 609–615.
108 https://doi.org/10.1530/jrf.0.0990609

109 Shibuya, M., 2011. Vascular Endothelial Growth Factor (VEGF) and Its Receptor (VEGFR) Signaling in
110 Angiogenesis. Genes Cancer 2, 1097–1105. https://doi.org/10.1177/1947601911423031

111 Silva, C.J.S. da, Simón, R., Busturia, A., 2018. Epigenetic and non-epigenetic functions of the RYBP protein
112 in development and disease. Mech. Ageing Dev. 174, 111–120. https://doi.org/10.1016/j.mad.2018.03.011

113 Simpson, R.A., Mayhew, T.M., Barnes, P.R., 1992. From 13 weeks to term, the trophoblast of human
114 placenta grows by the continuous recruitment of new proliferative units: A study of nuclear number using
115 the disector. Placenta 13, 501–512. https://doi.org/10.1016/0143-4004(92)90055-x

116 Singh, R., Wu, A.P., Mudide, A., Berger, B., 2024. Causal gene regulatory analysis with RNA velocity reveals
117 an interplay between slow and fast transcription factors. Cell Syst. 15, 462-474.e5.
118 https://doi.org/10.1016/j.cels.2024.04.005

119 Street, K., Risso, D., Fletcher, R.B., Das, D., Ngai, J., Yosef, N., Purdom, E., Dudoit, S., 2018. Slingshot: cell
120 lineage and pseudotime inference for single-cell transcriptomics. BMC Genom. 19, 477.
121 https://doi.org/10.1186/s12864-018-4772-0

122 Stuart, T., Butler, A., Hoffman, P., Hafemeister, C., Papalexi, E., Mauck, W.M., Hao, Y., Stoeckius, M.,
123 Smibert, P., Satija, R., 2019. Comprehensive Integration of Single-Cell Data. Cell 177, 1888-1902.e21.
124 https://doi.org/10.1016/j.cell.2019.05.031

Suryawanshi, H., Morozov, P., Straus, A., Sahasrabudhe, N., Max, K.E.A., Garzia, A., Kustagi, M., Tuschl, T., Williams, Z., 2018. A single-cell survey of the human first-trimester placenta and decidua. Sci Adv 4, eaau4788. https://doi.org/10.1126/sciadv.aau4788

Tuohey, L., Macintire, K., Ye, L., Palmer, K., Skubisz, M., Tong, S., Kaitu'u-Lino, T.J., 2013. PLAC4 is upregulated in severe early onset preeclampsia and upregulated with syncytialisation but not hypoxia. Placenta 34, 256–260. https://doi.org/10.1016/j.placenta.2012.12.009

Turco, M.Y., Gardner, L., Kay, R.G., Hamilton, R.S., Prater, M., Hollinshead, M., McWhinnie, A., Esposito, L., Fernando, R., Skelton, H., Reimann, F., Gribble, F., Sharkey, A., Marsh, S.G.E., O'Rahilly, S., Hemberger, M., Burton, G.J., Moffett, A., 2019. Trophoblast organoids as a model for maternal-fetal interactions during human placentation. Nature 564, 263–267. https://doi.org/10.1038/s41586-018-0753-3

Turco, M.Y., Moffett, A., 2019. Development of the human placenta. Development 146, dev163428. https://doi.org/10.1242/dev.163428

Van den Berge K, Roux de Bezieux H, Street K, Saelens W, Cannoodt R, Saeys Y, Dudoit S, Clement L. Trajectory-based differential expression analysis for single-cell sequencing data. Nat Commun. 2020;11(1):1201. https://doi.org/10.1038/s41467-020-14766-3

Vento-Tormo, R., Efremova, M., Botting, R.A., Turco, M.Y., Vento-Tormo, M., Meyer, K.B., Park, J.-E., Stephenson, E., Polański, K., Goncalves, A., Gardner, L., Holmqvist, S., Henriksson, J., Zou, A., Sharkey, A.M., Millar, B., Innes, B., Wood, L., Wilbrey-Clark, A., Payne, R.P., Ivarsson, M.A., Lisgo, S., Filby, A., Rowitch, D.H., Bulmer, J.N., Wright, G.J., Stubbington, M.J.T., Haniffa, M., Moffett, A., Teichmann, S.A., 2018. Single-cell reconstruction of the early maternal–fetal interface in humans. Nature 563, 347–353. https://doi.org/10.1038/s41586-018-0698-6

Wang, M., Liu, Y., Sun, R., Liu, F., Li, J., Yan, L., Zhang, J., Xie, X., Li, D., Wang, Y., Li, S., Zhu, X., Li, R., Lu, F., Xiao, Z., Wang, H., 2024. Single-nucleus multi-omic profiling of human placental syncytiotrophoblasts identifies cellular trajectories during pregnancy. Nat. Genet. 56, 294–305. https://doi.org/10.1038/s41588-023-01647-w

Wooding, P., Burton, G., 2008. Comparative Placentation, Structures, Functions and Evolution. https://doi.org/10.1007/978-3-540-78797-6

Yang, L., Liang, P., Yang, H., Coyne, C.B., 2023. Trophoblast organoids with physiological polarity model placental structure and function. J. Cell Sci. 137, jcs261528. https://doi.org/10.1242/jcs.261528

Yang, L., Semmes, E.C., Ovies, C., Megli, C., Permar, S., Gilner, J.B., Coyne, C.B., 2022. Innate immune signaling in trophoblast and decidua organoids defines differential antiviral defenses at the maternal-fetal interface. eLife 11, e79794. https://doi.org/10.7554/elife.79794

Zappia L, Oshlack A. Clustering trees: a visualization for evaluating clusterings at multiple resolutions. Gigascience. 2018;7(7). http://doi: 10.1093/gigascience/giy083.

Zeltz, C., Gullberg, D., 2016. The integrin–collagen connection – a glue for tissue repair? J. Cell Sci. 129, 1284–1284. https://doi.org/10.1242/jcs.188672

Zhu, Y.-N., Pan, F., Gan, X.-W., Liu, Y., Wang, W.-S., Sun, K., 2023. The Role of DNMT1 and C/EBPα in the Regulation of CYP11A1 Expression During Syncytialization of Human Placental Trophoblasts. Endocrinology 165, bqad195. https://doi.org/10.1210/endocr/bqad195